MOTILE ORGANISMS DISPERSING AND TRACKING CHEMICAL SIGNALS

A DISSERTATION SUBMITTED TO THE GRADUATE DIVISION OF THE UNIVERSITY OF HAWAI'I AT MĀNOA IN PARTIAL FULFILLMENT OF THE REQUIREMENTS FOR THE DEGREE OF

DOCTOR OF PHILOSOPHY

IN

MATHEMATICS

DECEMBER 2019

By

Don A. Krasky

Dissertation Committee:

Daisuke Takagi, Chairperson
Monique Chyba
Sara Post
Yuriy Mileyko
Sangwoo Shin

ACKNOWLEDGMENTS

The guidance provided by Dr. Takagi throughout this project has been invaluable, and none of this would have been possible without him. He has provided support of a mentor, and never made me feel I was incapable of completing my project. Kenny Corea for listening to me babble about these projects for years and providing feedback. My parents for raising me in an environment that encouraged me to follow my dreams.

The ARO and NSF have been good to me, their support has allowed me to eat and sleep in a relatively comfortable apartment while I was preparing this manuscript.

This work was supported by the US ARO Grants W911NF-15-1-0608 and W911NF-17-1-0442.

ABSTRACT

In this dissertation we draw inspiration from natural systems, and discuss some mathematical models inspired by them. With the goal of describing the motility of copepods, a model typically used to describe bacterial dispersion is extended. From a static diffusion constant and some statistics on velocity, the model provides an effective diffusion constant in the n-dimensional Cartesian space $\mathbb{R}^n$. We then explore interactions between organisms. Chemical signals are described mathematically for stationary and moving sources. The results describe how detecting and signaling organisms are likely to pair up based on motility. Both sections apply mathematical ideas to biological systems, taking a few simple assumptions and discussing their consequences.

We introduce a model for dispersion of independent swimmers jumping randomly between multiple translational velocities in arbitrary dimensions. Sample trajectories of the individual swimmers are simulated using the governing stochastic differential equations. The associated Fokker-Planck equations are derived and an analytic prediction is obtained for the effective diffusion constant, which is shown to be consistent with simulations. We show adaptability of the model by fitting to three previous models of swimmers having two or three preferred velocities. We explore how stochastic vs. deterministic velocity changes and restricting certain velocity jumps result in different rates of dispersion.

Chemical signals are present over a wide range of scales in nature, from as small as being inhabited by bacteria, all the way up to salmon tracking their home stream in the open ocean. These signals can alert organisms in the presence of predators, help locate food resources, or aid in the effort to find mates. Evolution has had the chance to optimize the motility and sensitivity of organisms to best exploit chemical signals. However, detection is still only possible down to a certain concentration threshold. Motivated by bacteria searching for food patches in a heterogeneous environment we provide calculations to describe the detectable region of a diffusing nutrient patch. From this, a critical chemotactic velocity necessary to reach the origin of the patch can be obtained. Motility is seen to provide additional information only in a donut-shaped region around the source. We then change focus to a moving source. Our calculations show that in ideal conditions access to concentration gradient and sufficient mobility guarantee the ability to find the source once it is detected. Descriptive formulae are provided for the dimensions and shape of the trailing plume from a given release rate and minimum detectable concentration. We discuss optimum types of

chaser/source match-ups and provide relevant descriptive calculations. We then apply our results to real world scenarios, demonstrating the usefulness and coherence of our work.

CONTENTS

LIST OF TABLES

LIST OF FIGURES

CHAPTER 1
INTRODUCTION

1.1 General Background

This dissertation contains the cumulative effort of 3 years work under the supervision of Dr. Daisuke Takagi. The chapter on diffusion of swimmers was presented at last years APS March Meeting in Boston, and the newer work on chemical sensing will be published in the near future. I have enjoyed learning about the current state of mathematical diffusion models in Biology, and feel privileged to have had the opportunity to provide a contribution to human knowledge. For every page of this work there is a stack of scratch paper full of failed attempts and incorrect information. If not for the optimism and mentorship of Dr. Takagi those scattered notes may have never been organized into a coherent format.

Motivation for this work stems from research and observations by Dr. Takagi's lab group. When I joined his research group the projects were all focused on modelling motility and sensory capabilities of copepods. Graduate students Davide DeVine and Rintaro Hayashi were working on detailed models of how leg movement was translated into movement. Undergraduate students were analyzing videos of leg motion, tracking swim trajectories, and analyzing models of sensory systems. After some discussion Dr. Takagi suggested that my first project should look into group behavior of copepods, focusing on obtaining a diffusion constant.

1.2 Motile Organisms Dispersing

Locomotion and dispersal are important processes that affect the distribution and abundance of organisms. Organisms swimming at a characteristic speed U and reorienting at a characteristic time T are expected to disperse with an effective diffusion constant in the order of U^2/T, which can be orders of magnitude greater than the diffusion constant purely due to Brownian motion [5, 46, 54]. Observations of bacteria and zooplankton such as Daphnia and copepods show that microscopic swimmers can spontaneously and dramatically change their translational and angular velocities [49, 44, 32]. These organisms and other biological and engineered systems of self-propelled particles have inspired a wide variety of works investigating the effects of directional changes [49, 40, 62, 25, 55, 57],

sudden velocity changes [44, 32, 10, 59, 42, 1, 24], or a combination of general velocity and directional changes [53, 15, 16]. These references demonstrate that short-term movements of individuals can profoundly influence their long-term dispersal behavior.

Laboratory observations of swimming organisms commonly produce velocity distributions with peaks around a few values [49, 44, 32, 40, 59]. A model specifically tailored for sudden changes between any number of velocities would offer valuable physical intuition into the dispersal of various organisms from small to large time scales. For example, observations of larval copepods show repeated reversals of velocity resulting in jagged edged, jiggling trajectories over small time scales [44], while over larger time scales they show richer behavior as they transition between multiple different velocities, experiencing periods of resting, coasting at slow speeds, and escaping or sprinting at high speeds. A model that incorporates any number of velocities may be able to account for all of these behaviors and predict how they affect the overall diffusivity.

We will derive a simple formula for the diffusivity of swimmers experiencing sudden changes in velocity in arbitrary dimensions. The formula shows that the diffusivity with multiple velocities is not equal in general to that of a swimmer moving at the average velocity. We demonstrate the flexibility of our model by comparing our results with three specific models of swimmers jumping between two or three velocities as considered previously [32, 59, 42]. Our comparisons either show an exact match under equivalent conditions, or result in a relatively small error. The comparisons provide an opportunity to discuss the effects of restricting certain changes between velocities or using a deterministic scheme for the velocity changes.

Organisms have been assumed to act passively, independent of each other and their environment. Anyone who has watched animal planet knows this is not the case. Environmental cues guide the behaviors of organisms. Next we examine the production and detection of chemical signals by the organisms with the goal of eventually adding changes in response to environmental ques to the diffusion model.

1.3 Motile Organisms Tracking Chemical Signals

Sensing and signaling are ubiquitous in nature. At large scales salmon follow a chemical signature from their birth stream [47] [63], moths signal their location to potential mates [64] [11], and harbor seals track hydrodynamic wakes left by fish [14] [26]. At intermediate scales settling snail larvae

use plumes above reefs to select optimum areas to settle and mature [39]. At much smaller scales copepods track mates [31] [17] [2] [36] [35] [61] [64] [65] and bacteria use chemotaxis to find patches of concentrated nutrients caused by lysed cells, flagellate excretions, sloppy feeding, or organic seeps [38] [7] [30] [27] [51] [37] [56]. General background on signaling and modeling techniques for these scenarios are reviewed in [47] [6] [5] [12]. We will not focus on the sensory apparatus or minute details of the signal, but rather the relationships between motility, sensed concentration gradients, and where these gradients can be detected. Our development will apply directly to laminar flow regimes, and to mean concentration fields in higher Reynolds number applications. In the paradigm outlined in [48] we will discuss navigation based on an internal state only, leaving the questions of how organisms move to other works.

Crabs, moths, and salmon have access to sensory information about ambient flow that help guide their movements [64] [28]. In contrast, bacteria and copepods track chemical signals in the absence of light or current [30] [65] [17]. As we wish to examine only the effects of the chemical signal we have drawn our motivation and background information from works involving these two groups of organisms. Our analysis will focus purely on the detectability and available information from a chemical signal rather than the fluid dynamics of the surrounding medium, which often complicates analysis enough to require numerical solutions. The goal here is to take a simple approach with easily interpretable analytic solutions. To this end our models treat organisms as points that do not cause secondary concentration profile changes due to fluid interaction in their immediate surroundings.

The survival of bacteria depends on extracting nutrients from their local environment. They can either count on diffusion, or actively transport themselves to nutrient rich zones [56] [7] [37]. While energetically expensive, chemotaxis has been roughly estimated to increase uptake by 50% [7] [58]. Our model is motivated by a bacterium attempting to feed on the results of a nearby cell lysing, which we approximate as an instantaneous chemical release at a point. Just after release the chemical signal would be too weak to detect. Over time the bacterium would experience a sudden increase in concentration, which would then slowly decrease back to background levels. If the bacterium is close enough it will notice this increase, then take advantage of its motility to reach the most concentrated region. For a short period, motion gives the bacterial additional information in a donut shaped region around the source that may aid in navigation. A change in variables then provides a nice segue to formulae describing a moving source continually releasing chemicals.

The abundance of copepods has resulted in a great body of literature [31] [2] [30] [17]. Greater

than 20 species of copepod have been shown to use pheromone tracking to find mates, the majority of which track long and slender trails left by cruising females. Copepods have also been observed to follow larger chemical trails left by sinking marine snow [23] [37] [45]. We model these scenerios as a moving source continuously releasing a chemical tracer. For a chaser to have a chance at finding the source it must move at a faster rate. This is seen to guarantee capture if the trail is continuously deposited in a straight line. It turns out this is not the case for copepods, which have been observed to fail approximately 50% of the time [17]. We discuss possible causes for these errors and the zig-zagged path often taken by chasing organisms. This leads nicely to a discussion of optimum pairings for effective signaling.

Different chaser and source pairs will have different formulae better suited to describe encounter rates. Encounters based on signaling have been described classically in [22], which concludes that fast moving predators are better suited at harvesting slow moving prey, and slow moving ambush predators are better suited to fast moving prey. This is surmised by using a sphere as an organisms detectable region. Since our discussion gives a more detailed analysis of chemical signaling, we discuss more appropriate figures to describe encounter zones for different predator-prey pairings. After this discussion we apply our results to some real world examples to demonstrate utility and adaptability of our work.

1.4 Main Idea: Continuity Equation

Suppose that for all positions $x \in \mathbb{R}^n$ and times t we have a concentration distribution given by an integrable function $\psi(x,t)$. For any region $E \in \mathbb{R}^n$ and flux $F : \mathbb{R}^n \mapsto \mathbb{R}^n$ we have a continuity equation that states the change over time of concentration in E is opposite the amount of measured quantity leaving E. Formally, with $\underline{n}$ as the outward normal vector to E, this looks like

$$\begin{aligned} \frac{\partial}{\partial t}\int_E \psi dV = -\oint_{\partial E}(F\cdot \underline{n})dS = -\int_E \nabla\cdot F dV \\ \implies \int_E (\frac{\partial}{\partial t}\psi + \nabla\cdot F)dV = 0. \end{aligned} \tag{1.1}$$

We have taken advantage of the divergence rheorem in the first line. Since the region E was arbitrary we have

$$\frac{\partial}{\partial t}\psi + \nabla\cdot F = 0. \tag{1.2}$$

Equation 1.2 will be the backbone of all analysis in this paper. When talking about chemicals diffusing without background flow we have Fick's Law, which states flux is proportional to and opposite direction of concentration gradient,

$$F = -D\nabla\psi(x,t). \tag{1.3}$$

For diffusing chemicals in a steady background flow with direction $u \in \mathbb{R}^n$ we have an additional advection term,

$$F = u\psi(x,t) - D\nabla\psi(x,t), \tag{1.4}$$

which results in the Advection-Diffusion equation. For active Brownian swimmers with velocity given by a function $u(x,t)$ we have

$$F = u(x,t)\psi(x,t) - D\nabla\psi(x,t), \tag{1.5}$$

which results in a Fokker-Planck equation describing the distribution of swimmers.

CHAPTER 2
DIFFUSION OF SWIMMERS JUMPING STOCHASTICALLY BETWEEN MULTIPLE VELOCITIES

2.1 Assumptions

There are several key assumptions underlying our model. We assume swimmers jump between multiple states via a Poisson process. Swimmers have no memory of their last change. Rather, future dynamics depend only on the swimmers' current state. When a jump occurs the swimmer has equal probability of landing in every other state. As a consequence each state is expected to have an equal population in the long term. If change statistics were depicted as a directed graph with nodes as states it would be fully connected. Despite these assumptions the model can attain any rational swim velocity probability distribution by assigning to multiple states the same velocity. This allows for analysis of run-and-tumble behavior consisting of alternating between a long run and a brief tumble, or a three-speed swimmer with unequal proportions of time moving at each speed [32]. Any long-term probability distribution of the swimming velocity can be approximated as finely as desired by adding more and more states to the model. While transition statistics cannot be matched in general, we show that by matching average escape rates a reasonable approximation for the diffusion constant can be obtained for any application that may arrive. We include independent noise terms for both position and orientation, which can be tuned to fit applications. From these assumptions we derive an analytic solution for the mean square displacement and show accuracy by comparing with simulations of active swimmers.

2.2 Theoretical Background

The general stochastic differential equation describing active Brownian motion of a single swimmer. Here W_t denotes the standard Weiner process as a vector of independent instances of mean zero unit variance gaussian distributions. The equation

$$dx = b\ dt + \sigma\ dW_t \tag{2.1}$$

describes deterministic changes in position, b, and random fluctuations due the swimmers interaction with the environment, σ. From this we can derive a Fokker-Planck, or forward Kolmogorov, equation describing how the probability distribution of swimmers changes over time. From the development in [52] we have for the pdf $\psi(x,t)$ describing the probability of finding a swimmer at x at time t the evolution equation

$$\frac{\partial}{\partial t}\psi = \nabla \cdot (-b\ \psi + \nabla \cdot (\sigma\sigma^T \psi)). \tag{2.2}$$

If the individual swimmers trajectories can be written in Langevin form $\dot{x} = u(t) - D\nabla \log \psi$ then the Fokker-Planck equation takes a simpler form,

$$\frac{\partial}{\partial t}\psi = \nabla(\dot{x}\psi). \tag{2.3}$$

2.3 Equations of Motion & Simulations

Our model tracks both the position in n-dimentional space, $x \in \mathbb{R}^n$, and orientation, $p \in \mathbb{S}^{n-1}$, of swimming organisms under the effects of Brownian motion. We denote their translational diffusivity by D, and rotational diffusivity by D_r. For a specific fluid and swimmer shape these constants can be calculated based on Brownian potential and temperature; we refer the interested reader to [18]. In the absence of swimming we expect mean square displacement to grow linearly with time as $2nDt$ in $\mathbb{R}^n$ and the reorientation time scale to be $\frac{1}{(n-1)D_r}$. Each organism changes randomly between m states. A swimmer in state i swims at a speed U_i with direction p. We assume our swimmer changes state via a memoryless exponentially distributed Poisson process with rate parameter f. This scheme guarantees future dynamics depend only on the current state of the swimmer. A two-dimensional example of this scheme with two states is sketched in figure 2.1.

With the constants above, the resulting dynamics in arbitrary dimensions are governed by the stochastic differential equation (SDE)

$$d\begin{bmatrix} x \\ p \end{bmatrix} = \begin{bmatrix} U_i p \\ 0 \end{bmatrix} dt + \begin{bmatrix} \sqrt{2D}\cdot I & 0 \\ 0 & \sqrt{2D_r}\cdot(I - pp^T) \end{bmatrix} dW_t, \tag{2.4}$$

where W_t denotes a vector of independent Weiner processes [52]. Here we have assumed our swimmers to be spherical. One could create a similar equation to describe more realistic swimmer ge-

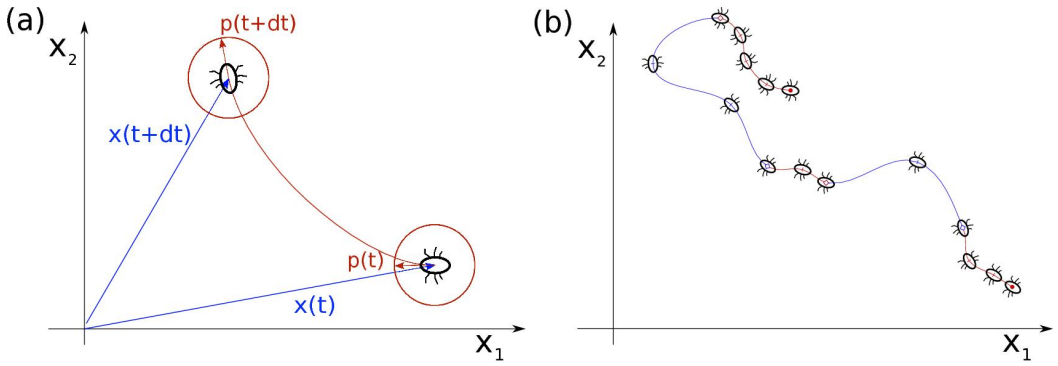

Figure 2.1: (a) A sketch of the position vector x and orientation vector p as they vary over time. (b) A typical two-speed trajectory with speed denoted by color: slower speed in red, and faster in blue.

ometry, however the symmetry from assuming spherical swimmers in the noise matrix makes the transition to a Fokker-Planck equation doable by hand.

To simulate ensembles of swimmers in two dimensions we adapt equation 2.4 to two dimensions and two states. Using polar coordinates, θ describes the orientation of the swimmer with respect to the x_1-axis. Particle motion is then described by

$$d\begin{bmatrix} x_1 \\ x_2 \\ \theta \end{bmatrix} = \begin{bmatrix} U_i \cos(\theta) \\ U_i \sin(\theta) \\ 0 \end{bmatrix} dt + \begin{bmatrix} \sqrt{2D} & 0 & 0 \\ 0 & \sqrt{2D} & 0 \\ 0 & 0 & \sqrt{2D_r} \end{bmatrix} dW_t. \tag{2.5}$$

In our simulations swimmers were initialized at the origin. Euler's method was used to approximate individual paths with a fixed time step $\Delta t = 0.1$. At each step Gaussian random variables ξ_x, ξ_y, ξ_θ are added in accordance with (2.5) to account for noise terms. Another random variable χ distributed uniformly in $[0, 1]$ is used to determine when changes in speed occur. At each iteration χ is compared with $f\Delta t$ to determine whether speed changes at the next step. If $\chi < f\Delta t$ a change in speed is made, otherwise speed remains the same.

Some sample trajectories generated under this scheme are shown in figure 2.2. Each panel contains a representative trajectory and a shaded circle expected to contain half of such particles after 50 time steps. Open circles denote locations where state changes have occurred. The values of $U_1 = 1$, $D_r = 0.1$, and $f = 0.2$ are fixed while the alternate speed, U_2, is set to a different value in each panel. In panel a, $U_2 = 1$, the swimmer maintains constant speed without reversing direction. This results in maximum diffusion. In panel b, $U_2 = -1$, the swimming direction reverses without

changing speed. In panel c, $U_2 = -1/3$, the direction reverses simultaneously with a speed change by a factor of three. This setup results in the smallest non-stationary diffusion with the set parameters (see figure 2.4).

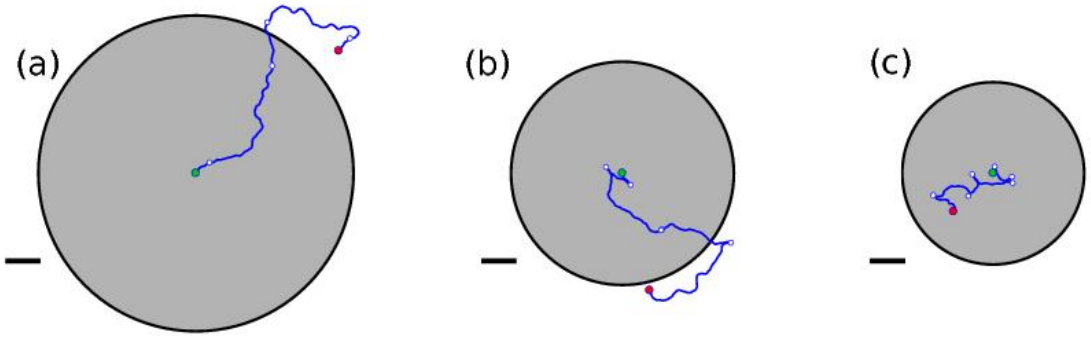

Figure 2.2: Sample trajectories of two-state swimmers starting at the green dot and ending at the red dot after 50 time steps. Open circles represent state changes with (a) no change in direction or speed; (b) direction reversal but no speed change; (c) direction reversal and speed changing by a factor of 3. Large circles shaded in gray show the areas expected to contain half of the swimmers. Scale bars are equivalent and represent 5 units of distance.

2.4 Analytic Model

To gain insight into the statistical properties of a large collection of swimmers, we develop an accompanying analytic model based on the Fokker-Planck equation associated with the corresponding Langevin dynamics. The stochastic process described above gives us information about the probability of finding a swimmer in state i (moving at speed U_i) at position x, with orientation p, at time t, with state jump rate f. We represent this information with the probability density function $\psi(x,p,t) = \sum_{i=1}^{m} \psi_i(x,p,t)$. The split of ψ into m separate functions is done so that each state has its own partition of ψ. While ψ is a proper probability distribution function, each ψ_i only describes a portion of the population and thus does not integrate to one over space. The main pdf obeys the Fokker-Planck equation

$$\frac{\partial \psi}{\partial t} + \nabla_x(\dot{x}\psi) + \mathscr{R}(\dot{p}\psi) = 0, \tag{2.6}$$

where ∇_x is the gradient constrained to x, $\mathscr{R} = (I - pp^T)\nabla_p$ is the gradient operator on p constrained to the unit sphere. Since this equation is linear in ψ, so we can split equation (2.6) to include

information on change statistics between states. The functions ψ_i evolve according to the Fokker-Planck equations

$$\frac{\partial \psi_i}{\partial t} + \nabla_x(\dot{x}\psi_i) + \mathscr{R}(\dot{p}\psi_i) = -f\psi_i + \frac{1}{(m-1)} \sum_{i \neq j \& j=1}^{m} f\psi_j \tag{2.7}$$

Summing these equations over m gives equation (2.6) as the terms on the right side cancel. With the inclusion of the Langevin dynamics

$$\begin{aligned} \dot{x} &= U_i p - D\nabla_x \ln(\psi_i) \\ \dot{p} &= -D_r \mathscr{R} \ln(\psi_i) \end{aligned} \tag{2.8}$$

the governing equations (2.7) reduce to

$$\frac{\partial \psi_i}{\partial t} = D\nabla_x^2 \psi_i - U_i \nabla_x p \psi_i + D_r \mathscr{R}^2 \psi_i - f\psi_i + \frac{1}{(m-1)} \sum_{i \neq j \& j=1}^{m} f\psi_j. \tag{2.9}$$

At this point the reader may question why we have chosen to omit any deterministic directional changes. The answer is that in equation 2.9 derivatives with respect to orientation are all of second order, and thus point in the opposite direction of p instead of in the tangent plane to the unit sphere. Including a turn distribution also includes first derivatives in equation 2.9, which makes the pen and paper calculation of integrals difficult.

With this formulation we have assumed swimmers have equal long-term probability of being in each state. This may seem restrictive, however multiple states may be assigned the same speed. This achieves uneven velocity proportions, while maintaining equal state populations. For example, If we wish to model run-and-tumble behavior with our swimmer being active $\frac{2}{3}$ of the time, we use three states, with $U_1 = U_2 = U$, the swimming speed, and $U_3 = 0$. This will mean a swimmer at velocity U will, at the next state change, either continue swimming at speed U, or stop and tumble with equal probability. However a tumbling swimmer is guaranteed to swim at speed U after the next state change.

We now find an analytic expression for the mean square displacement

$$\langle x \cdot x \rangle(t) = \int (x \cdot x)(\sum_{j=1}^{m} \psi_j) dx dp. \tag{2.10}$$

Differentiating with respect to t and using (2.9), we obtain

$$\begin{aligned}
&\frac{d}{dt}\langle x\cdot x\rangle = \frac{d}{dt}\int_{\mathbb{R}^n\times\mathbb{S}^{n-1}}(x\cdot x)\psi dxdp\\
&=\int_{\mathbb{R}^n\times\mathbb{S}^{n-1}}(x\cdot x)\frac{d}{dt}\psi dxdp\\
&=\int_{\mathbb{R}^n\times\mathbb{S}^{n-1}}(x_kx_k)\sum_{i=1}^{m}(D\nabla_x^2\psi_i - U_ip\nabla_x\psi_i + D_r\mathscr{R}^2\psi_i - f\psi_i + \frac{1}{(m-1)}\sum_{j\neq i\&j=1}^{m} f\psi_j)dxdp.
\end{aligned} \tag{2.11}$$

Here equation (2.7) has been applied. We then proceed with integration by parts, requiring that ψ and all its derivatives approach zero for large $|x|$ and t. This gives

$$\begin{aligned}
&=\int_{\mathbb{R}^n\times\mathbb{S}^{n-1}} 2nD\psi + 2x_kp_kU_i\psi_i + 0\ dxdp\\
&=2nD+\sum_{i=1}^{m}2U_i\langle x\cdot p\rangle_i,
\end{aligned} \tag{2.12}$$

which has been expressed as a function of $\langle x\cdot p\rangle_i = \int(x\cdot p)\psi_i dxdp$.

To solve for $\langle x\cdot p\rangle_i$ we repeat the process used to compute (2.11),

$$\begin{aligned}
&\frac{d}{dt}\langle x\cdot p\rangle_i = \int_{\mathbb{R}^n\times\mathbb{S}^{n-1}}(x\cdot p)\frac{d}{dt}\psi_i dxdp\\
&=\int_{\mathbb{R}^n\times\mathbb{S}^{n-1}}(x_kp_k)(D\nabla_x^2\psi_i - U_ip\nabla_x\psi_i + D_r\mathscr{R}^2\psi_i - f\psi_i + \frac{1}{(m-1)}\sum_{j\neq i\&j=1}^{m} f\psi_j)dxdp\\
&=\int_{\mathbb{R}^n\times\mathbb{S}^{n-1}} -Dp_k\partial_{x_k}\psi_i + U_i(p_kp_k)\psi_i - D_rx_k(\mathscr{R}p)_k\mathscr{R}\psi_i - fx_kp_k\psi_i + \frac{1}{(m-1)}\sum_{j\neq i\&j=1}^{m}.fx_kp_k\psi_j dxdp
\end{aligned} \tag{2.13}$$

We have applied equation 2.7, and done an integration by parts. After another integration by parts and an application of boundary conditions we get

$$\begin{aligned}
&=\int_{\mathbb{R}^n\times\mathbb{S}^{n-1}} 0 + U_i\psi_i + D_r\psi_ix_k(\mathscr{R}^2p)_k - fx_kp_k\psi_i + \frac{1}{(m-1)}\sum_{j\neq i\&j=1}^{m} fx_kp_k\psi_j dxdp\\
&=U_i\langle 1\rangle_i - (n-1)D_r\int_{\mathbb{R}^n\times\mathbb{S}^{n-1}} x_kp_k\psi_i dxdp - f\langle x\cdot p\rangle_i + \frac{1}{m-1}f\sum_{j\neq i\&j=1}^{m}\langle x\cdot p\rangle_j\\
&=-((n-1)Dr+f)\langle x\cdot p\rangle_i + \frac{1}{m-1}f\sum_{j\neq i\&j=1}^{m}\langle x\cdot p\rangle_j + U_i\langle 1\rangle_i.
\end{aligned} \tag{2.14}$$

We have used the fact that $(\mathscr{R}^2 p)_k = -(n-1)p_k$, which can be seen since

$$\begin{aligned}(\mathscr{R}^2 p)_k &= (\delta_{ij} - p_i p_j)\partial_{p_j}(\delta_{ik} - p_i p_k)\partial_{p_k} p_k \\ &= (\delta_{ij} - p_i p_j)\partial_{p_j}(\delta_{ik} - p_i p_k) \\ &= \partial_{p_i}(1 - p_i p_k) - p_i p_j \partial_{p_i}(1 - p_i p_k) \\ &= -np_k - p_k + p_k + p_k \\ &= -(n-1)p_k.\end{aligned} \tag{2.15}$$

From equation (2.13) the linear system of ODEs follows:

$$\frac{d}{dt}\begin{bmatrix} \vdots \\ \langle x \cdot p \rangle_i \\ \vdots \end{bmatrix} = A \begin{bmatrix} \vdots \\ \langle x \cdot p \rangle_i \\ \vdots \end{bmatrix} + \begin{bmatrix} \vdots \\ U_i \langle 1 \rangle_i \\ \vdots \end{bmatrix}. \tag{2.16}$$

Where the matrix A has elements

$$a_{i,j} = \begin{cases} -((n-1)D_r + f) & i = j \\ \frac{1}{(m-1)} f & i \neq j \end{cases} \tag{2.17}$$

for $i, j \in \{1, 2 \ldots, m\}$.

We peel back the onion one layer further to find $\langle 1 \rangle_i$ as a function of time. The same method as before applies, differentiate with respect to time and use the Fokker-Planck equation to integrate. This results in

$$\frac{d}{dt}\begin{bmatrix} \vdots \\ \langle 1 \rangle_i \\ \vdots \end{bmatrix} = \Phi \begin{bmatrix} \vdots \\ \langle 1 \rangle_i \\ \vdots \end{bmatrix} \tag{2.18}$$

Where the matrix Φ has elements

$$\phi_{i,j} = \begin{cases} -f & i = j \\ \frac{1}{(m-1)} f & i \neq j \end{cases} \tag{2.19}$$

for $i, j \in \{1, 2 \ldots, m\}$. The matrix Φ has eigenvectors and eigenvalue pairs

$$\begin{aligned} \zeta = 0,\ v_0 &= \begin{bmatrix} 1 \\ \vdots \\ 1 \end{bmatrix}, \\ \nu = -\frac{mf}{(m-1)},\ v_i &= \begin{bmatrix} \frac{1}{m-1} \\ \vdots \\ \frac{1}{m-1} \\ -1 \\ \frac{1}{m-1} \\ \vdots \\ \frac{1}{m-1} \end{bmatrix}. \end{aligned} \tag{2.20}$$

Since the eigenvalue $\nu < 0$, all solutions decay to the stable solution $\langle 1 \rangle_i = \frac{1}{m}$ after approximate time $\frac{1}{f}$. At this point swimmers collective behavior is not influenced by initial state populations.

The form of the ODE (2.16) suggests a constant solution exists. We first find this solution and discuss the general solution later. Setting $\frac{d}{dt}\langle x \cdot p \rangle_i = 0$ and solving for $\langle x \cdot p \rangle_i$ we get

$$\begin{bmatrix} \vdots \\ \langle x \cdot p \rangle_i \\ \vdots \end{bmatrix} = -A^{-1} \begin{bmatrix} \vdots \\ \frac{1}{m} U_i \\ \vdots \end{bmatrix} \tag{2.21}$$

As A is symmetric and full rank it can be orthogonally diagonalized, with the form $A = BDB^T$. The matrix B is composed of orthonormal eigenvectors of A, and D is a diagonal matrix with

corresponding eigenvalues on the diagonal. Here are the eigenvalues and eigenvectors:

$$\alpha = -(n-1)D_r,\ v_0 = \frac{1}{\sqrt{m}}\begin{bmatrix}1\\ \vdots \\ 1\end{bmatrix},$$
$$\beta = -((n-1)D_r + \frac{m}{m-1}f),\ v_i = \frac{1}{\sqrt{(m-i)(m-i+1)}}\begin{bmatrix}0\\ \vdots \\ 0\\ -(m-i)\\ 1\\ \vdots \\ 1\end{bmatrix}. \tag{2.22}$$

In the eigenvector v_i the term $-(m-i)$ occurs in the i'th row. These eigenvectors are orthogonal as required, and have been normalized to unit length. The matrices B and D are given by $B = [v_0, \ldots, v_{m-1}]$, and $D = \text{diag}\{\alpha, \beta, \ldots, \beta\}$.

We now find $A^{-1} = BD^{-1}B^T$. Making use of symmetry, we find the off-diagonal and diagonal entries. Setting $i < j$ we have

$$\begin{aligned}(a^{-1})_{i,j} &= \frac{1}{\alpha m} - \frac{1}{\beta(m-i+1)} + \sum_{k=1}^{i-1}\frac{1}{\beta(m-k+1)(m-k)},\\ (a^{-1})_{i,i} &= \frac{1}{\alpha m} + \frac{m-i}{\beta(m-i+1)} + \sum_{k=1}^{i-1}\frac{1}{\beta(m-k+1)(m-k)}.\end{aligned} \tag{2.23}$$

Using the fact that we have a telescoping sum $\sum_{k=1}^{i-1}\frac{1}{\beta(m-k+1)(m-k)} = \frac{1}{\beta}\sum_{k=1}^{i-1}\frac{1}{(m-k)} - \frac{1}{(m-k+1)} = \frac{-(i-1)}{\beta m(m-(i-1))}$, we can simplify (2.23) a bit more;

$$\begin{aligned}(a^{-1})_{i,j} &= \frac{1}{\alpha m} + \frac{1}{\beta m} - \frac{2}{\beta(m-i+1)},\\ (a^{-1})_{i,i} &= \frac{1}{\alpha m} + \frac{m-i}{\beta(m-i+1)} - \frac{i-1}{\beta m(m-i+1)}.\end{aligned} \tag{2.24}$$

Since $\langle x \cdot p \rangle_i = \frac{1}{m} \sum_{k=1}^{m} (a^{-1})_{i,k} U_k$, we arrive at

$$\langle x \cdot p \rangle_i = \frac{1}{m^2} \frac{\alpha - \beta}{\alpha\beta} \sum_{k=1}^{m} U_k - \frac{1}{\beta m} U_i. \tag{2.25}$$

From here we could compute a general solution for each $\langle x \cdot p \rangle_i$ from the eigenvalues and eigenvectors of A. However, since the eigenvalues $\alpha, \beta < 0$ the exponential terms in the general solution are negligible after the largest of $\frac{1}{|\alpha|}$, $\frac{1}{|\beta|}$, or $\frac{1}{f}$ time units. The time scale $\frac{1}{|\alpha|}$ is associated with random reorientations, the time scale $\frac{1}{|\beta|}$ is associated with both orientation and state memory loss, and the time scale $\frac{1}{f}$ relates to normalization of state populations. After time has passed the larger of the three, swimmers have no memory of their initial orientation or state. An effective diffusion constant describes the linear phase of mean squared displacement, after all of these fluctuations have disappeared. Since that is what we are after the additional calculation of an exact solution valid for all times is unnecessary. We can simply proceed with the constant solution found above. From (2.11) we deduce that after fluctuations due to initial conditions have dissipated $\langle x \cdot x \rangle(t) \approx 2nt(D + \frac{1}{n} \sum_{i=1}^{m} u_i \langle x \cdot p \rangle_i)$. Thus we have an effective diffusion coefficient

$$\begin{aligned} D_{eff} &= D + \frac{1}{n} \sum_{i=1}^{m} u_i \langle x \cdot p \rangle_i \\ &= D + \frac{1}{-\beta n m} \sum_{i=1}^{m} U_i^2 + \frac{1}{nm^2} \frac{\alpha - \beta}{\alpha\beta} (\sum_{i=1}^{m} U_i)^2. \end{aligned} \tag{2.26}$$

Setting all speeds to be equal, $U_i = U$, our formula reduces to the well known result $D_{eff} = D + \frac{U^2}{n(n-1)D_r}$. If we take $2m$ states, half at speed U_1 and half at speed U_2, we get a reduction to the case with two states, one at speed U_1, the other at speed U_2. There is, however, a correction factor for the change rate f. In the case with $2m$ states a transition in state corresponds with a change in velocity only m out of $2m - 1$ times, while in the two-state case a change in state guarantees a change in speed. This corrected jump rate is given by $f^* = \frac{m}{2m-1} f$.

To simplify verification against simulations we pass to a non-dimensional form of (2.26). First, we organize our equations so that $|U_1| \geq |U_2| \geq \ldots \geq |U_m|$. Then define $\tilde{U}_i = \frac{U_i}{U_1}$, and $\lambda = \frac{\alpha}{\beta} =$

$\frac{(n-1)D_r}{(n-1)D_r+\frac{m}{m-1}f}$. Using these substitutions we get

$$\begin{aligned} D_{eff} &= D - \frac{U_1^2}{n\alpha} \cdot d(\{\tilde{U}_i\}_{i=1}^m, \lambda), \\ d(\{\tilde{U}_i\}_{i=1}^m, \lambda) &= \lambda \frac{1}{m} \sum_{i=1}^{m} \tilde{U}_i{}^2 + (1-\lambda)\frac{1}{m^2}(\sum_{i=1}^{m} \tilde{U}_i)^2. \end{aligned} \tag{2.27}$$

As α is negative and $0 < \lambda \leq 1$ our additional diffusion is a multiple of the convex combination of a mean speed swimmer, and the case where the effective diffusion of swimmers in each state is averaged. This result cannot be achieved by simply taking the mean velocity of the swimmer and adding noise because different schemes with the same mean velocity still have effects from each individual velocity. Figure 2.3 shows that the diffusivity predicted by equation (2.27) agrees well with the diffusivity of two-state swimmers simulated at different λ, varied by adjusting f and keeping $D = 0$ and $D_r = 0.5$ fixed in the simulations. The effective diffusion of 50,000 swimmers, simulated over 1000 time steps, was computed via a linear regression run on mean square displacement over the last 900 steps to ignore initial ballistic diffusion.

2.5 Limiting Cases

For what follows we set $D = 0$ as it does not contribute to the interesting dynamics. As our jump rate $f \to 0$, we have $\lambda \to 1$, $d \to \frac{1}{m}\sum_{i=1}^{m} \tilde{U}_i{}^2$. This is the average diffusion taken over each state. It is consistent with intuition since we assumed each state starts with an equal number of swimmers. When the jump rate $f \to \infty$ we have $\lambda \to 0$. We find $d \to (\frac{1}{m}\sum_{i=1}^{m} \tilde{U}_i)^2$. Since switch rate is infinitely large, motion over any small time scale will include every possible state. This case corresponds to what we have called an 'average speed swimmer'.

Since $0 < \lambda \leq 1$ expected diffusion of a multi-speed swimmer is proportional to a convex combination of the above. Figure 2.4 shows added diffusion where we have fixed $D = 0$, $m = 2$, $U_1 = 1$, and $U_2 = U \in [0, 1]$. By symmetry these values capture all behavior of the model when restricted to two states. For fixed D_r and n, added effective diffusion is a constant multiple of height. The red curve describes the effective diffusion at $U = \frac{\lambda-1}{\lambda+1}$, the value of U that results in minimum added diffusion for fixed λ under the set parameters.

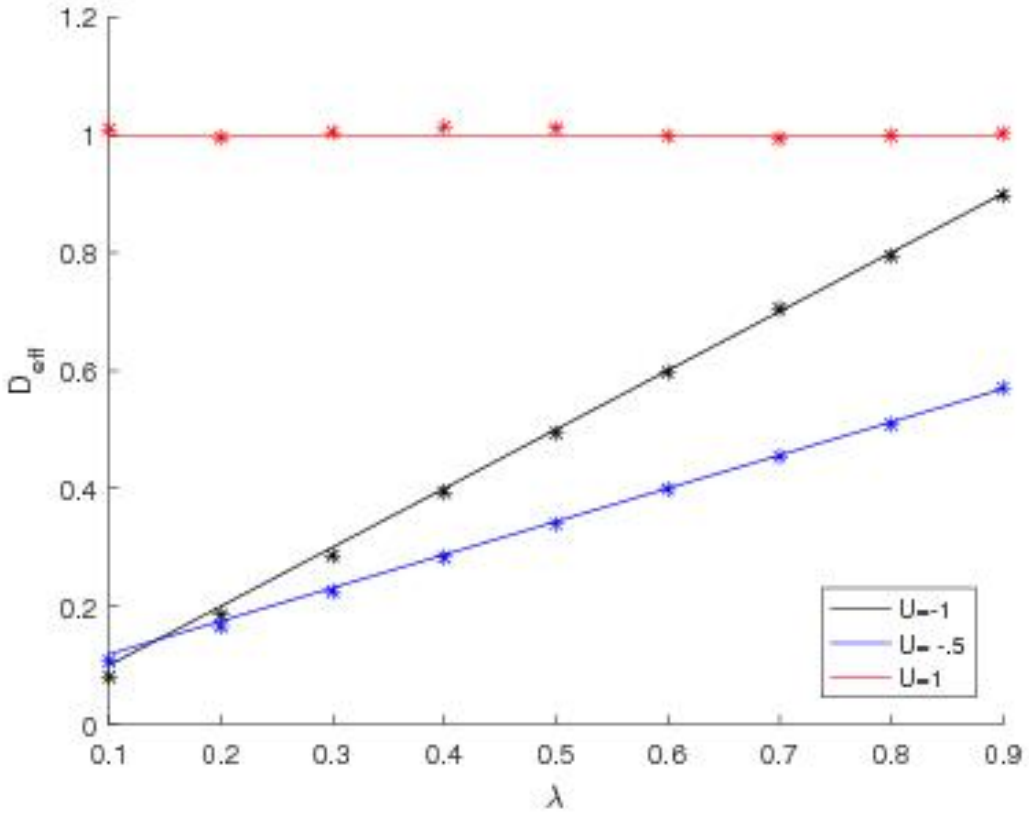

Figure 2.3: Comparison between predicted (lines) and simulated (symbols) diffusion constants of two-state swimmers with $U_1 = 1$ and $U_2 = U$.

2.6 Comparisons to Previous Work

In what follows we will show that, despite requiring equal state change rates and populations, our model can be adapted to fit a variety of applications. Some care must be taken when computing the change rate for each comparison; we give an example where this is done. We also compare with a deterministic switching scheme to observe how our assumption about random switching affects diffusivity.

Theves et al. [59] found an effective diffusion coefficient for a similar 3-d model with two randomly switching speeds of propagation. Let us call their effective diffusion D^S_{eff}. They assume exponentially distributed speed switch times, but have an extra directional persistence parameter we will call $\zeta = \langle \cos\phi \rangle$ where ϕ is the angle at which orientation changes with a change in speed. In our model

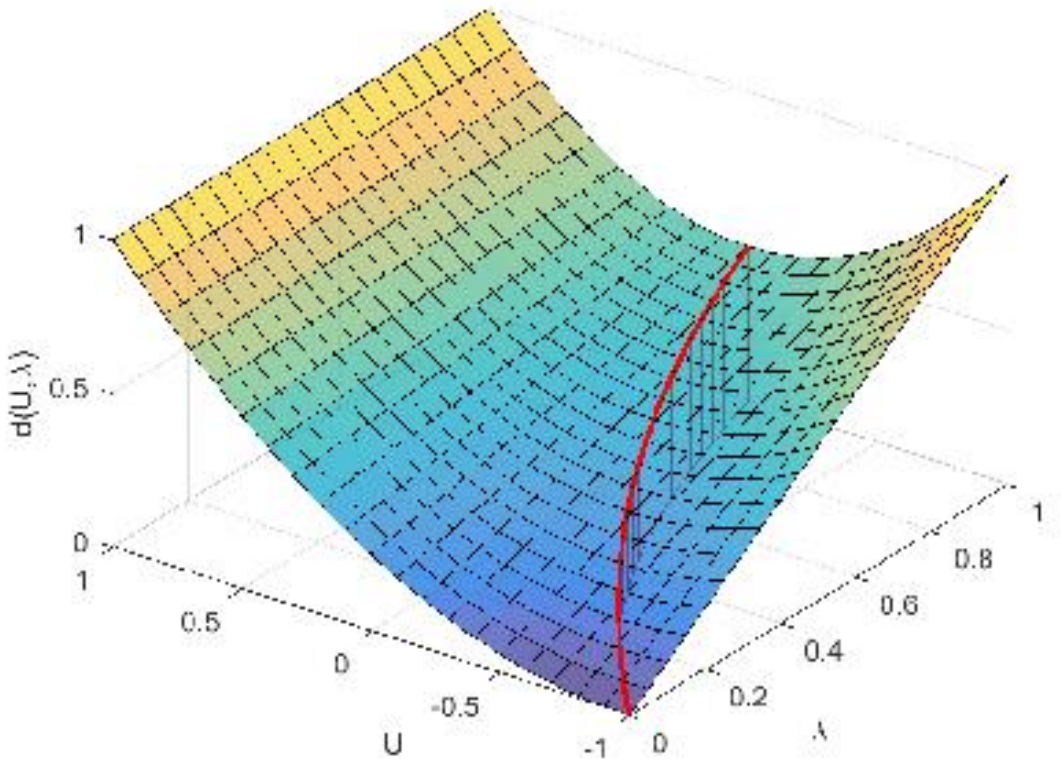

Figure 2.4: Added diffusion with two alternating speeds. One speed is fixed at 1 and the other is labeled U. For fixed D_r added effective diffusion is a constant multiple of height. The red curve describes the $U = \frac{\lambda-1}{\lambda+1}$ value that results in minimum added diffusion for fixed λ.

it is assumed that orientation does not change with speed jumps, so we set $\zeta = 1$. They report

$$D^S_{eff} = \frac{2D_r(U_1^2 + U_2^2) + f(U_1 + U_2)^2}{6(2D_r)(2D_r + 2f)}, \tag{2.28}$$

which has been translated to match our variable names. It is equivalent to our effective diffusion when $m = 2$, $n = 3$.

A deterministic switching scheme was used by Lauga [42], instead of a random one as employed in his paper. Let us call his effective diffusion D^D_{eff}. A speed $\bar{U}$ is chosen and the velocity alternates between $\bar{U}$ and $-\bar{U}$ at regular intervals of $\frac{\pi}{\omega}$, where ω is the rate parameter. He sets $\tau = \frac{1}{2D_r}$. In his notation the additional diffusion is $D^D_{eff} = \frac{\bar{U}^2\tau}{3}(1 - \frac{2\tau\omega}{\pi}\tanh(\frac{\pi}{2\tau\omega}))$, which translates to our notation

as

$$D^D_{eff} = \frac{U^2}{6D_r}(1 - 2\eta \tanh(\frac{1}{2\eta})) \tag{2.29}$$

where $\eta = \frac{f}{D_r}$. Our additional diffusion with direction reversals is $D_{eff} = \frac{U^2}{6D_r}\frac{1}{1+2\eta}$. Figure 2.5, normalized so that $D_{eff}, D^D_{eff} \to 1$ as $\eta \to 0$, shows that stochastic reversals result in faster diffusion than deterministic ones, and diffusion approaches zero much faster with switch rate in the deterministic case. This follows intuition as a deterministic swimmer will not have the occasional long run before a reversal.

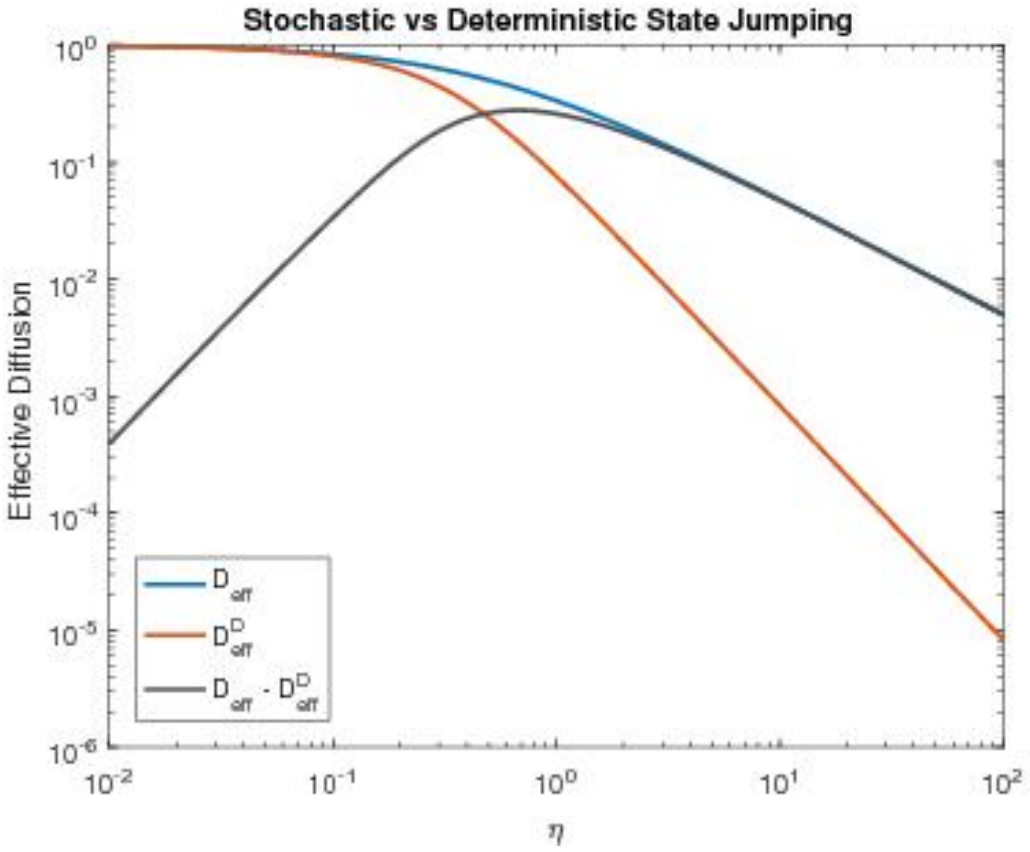

Figure 2.5: Comparison between stochastic reversals in our model and deterministic reversals considered by Lauga [42]. The effective diffusion is slightly higher with stochastic than deterministic reversals. The relative difference increases with larger switch rates between reversals.

A three-state 3-d model is considered by Hintsche et al. [32]. The swimmers are assumed to move at velocity U in state 1, $-U$ in state 2, and $\frac{-U}{2}$ in state 3. Changes are exponentially distributed with rate parameters described in figure 2.6, where $k \geq 0$ and $0 \leq p \leq 1$. Note that the directed graph representing transitions is not complete. For example the transition from $\frac{-U}{2}$ to $-U$ is not

allowed. Because of this we will call this scheme "restricted". Our adapted model results in a fully connected transition graph, shown in figure 2.7a. For this reason we will call our model "free". Let us label the restricted effective diffusion coefficient D^R_{eff}. With the parameters above

$$D^R_{eff} = \frac{U^2}{3(2+p)} \cdot \frac{16D_r(2D_r+k) + 4D_r(D_r+3k)p + k^2p^2}{8D_r(4D_r^2 + 6D_rk + k^2(2+p))}. \tag{2.30}$$

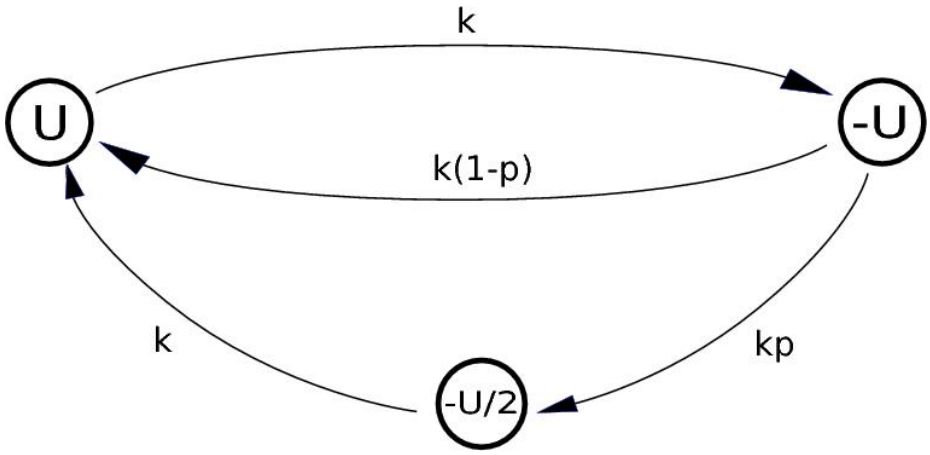

Figure 2.6: Exponential jump rate parameters for the restricted model proposed in [32]. Velocities are encircled and arrows are labeled with their respective change rate, with restrictions $k \geq 0$, $p \in [0, 1]$.

In the limiting case where $p \to 0$ the restricted model is reduced to two states with opposite speeds switching at rate k. The effective diffusion in this case, $D^R_{eff} = \frac{v_0^2}{6(D_r+k)}$, matches our model exactly with $n = 3$, $m = 2$, and $f = k$.

To compare models in a more interesting setting we compute a steady state distribution for the restricted model. To do this we set a small time increment Δt. Within Δt state transitions $U \to -U$ and $\frac{-U}{2} \to U$ happen with probability $a = 1 - e^{-k\Delta t}$, $-U \to U$ with probability $b = 1 - e^{-k(1-p)\Delta t}$, and $\frac{-U}{2} \to U$ with probability $c = 1 - e^{kp\Delta t}$. Letting s_1 have speed U, s_2 have speed $-U$, and s_3 have speed $-U/2$, the steady state distribution is given by the equation

$$\begin{bmatrix} 1-a & b & a \\ a & 1-b-c & 0 \\ 0 & c & -a \end{bmatrix} \begin{bmatrix} s_1 \\ s_2 \\ s_3 \end{bmatrix} = \begin{bmatrix} s_1 \\ s_2 \\ s_3 \end{bmatrix}$$

where s_1, s_2, and s_3 are the proportions of swimmers in each state, i.e. $s_1 + s_2 + s_3 = 1$. The solution

to this equation is

$$\begin{bmatrix} s_1 \\ s_2 \\ s_3 \end{bmatrix} = \frac{1}{a+b+2c} \begin{bmatrix} b+c \\ a \\ c \end{bmatrix} \rightarrow \begin{bmatrix} \frac{1}{2+p} \\ \frac{1}{2+p} \\ \frac{p}{2+p} \end{bmatrix} \text{ as } \Delta t \rightarrow 0.$$

To demonstrate how the restricted model can be approximated by our model by matching steady state distributions and average escape rates, we consider the simplest non-trivial case of $p = \frac{1}{2}$. This gives a steady state distribution of $\begin{bmatrix} s_1 \\ s_2 \\ s_3 \end{bmatrix} = \begin{bmatrix} 2/5 \\ 2/5 \\ 1/5 \end{bmatrix}$. Our adapted model will have $n = 3$ and $m = 5$. Two states (corresponding to s_1) will have speed U, two (corresponding to s_2) will have speed $-U$, and the final state (corresponding to s_3) will have speed $\frac{-U}{2}$. The change rates between states and corresponding velocites are presented in figure 2.7. Some care must be taken when choosing the

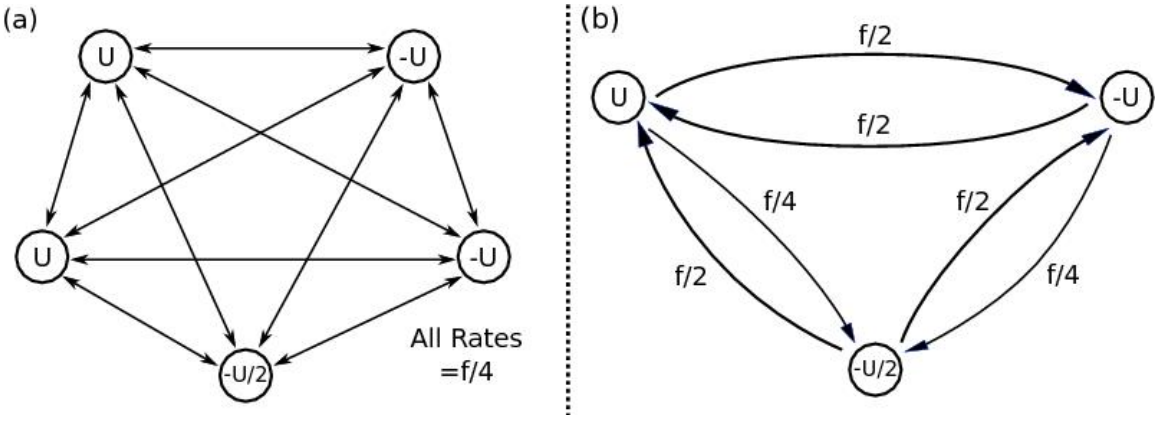

Figure 2.7: a.) 'Free' state changes for comparison with restricted changes in Figure 2.6. All rates are $f/4$. States are marked by circles with assigned velocities enclosed. b.) A compressed diagram displaying only velocities with change rates. In our comparison we set $k = \frac{4}{5}f$ to match the expected rate of changing velocities.

adapted change rate as not all transitions can be matched exactly. Instead we match the expected rate of changing velocities in the long run. In the restricted model the escape rate is k from every state. Thus, the expected rate of changing velocities is also k. For our adapted model, the rate of changing velocities from a state with velocity U or $-U$ is $\frac{3}{5}(\frac{f}{4})$, while the rate of changing from $-U/2$ is $\frac{4}{5}(\frac{f}{4})$. Accounting for the relative proportions of time being at each state, we obtain $\frac{4}{5}f$ as the expected rate of changing velocities. We match $k = \frac{4}{5}f$ and simplify comparison by introducing

a non-dimensional variable $\eta = \frac{f}{D_r}$. This gives the equations

$$\begin{aligned} D^R_{eff} &= \frac{17U^2}{120D_r} \cdot \frac{85 + 44\eta + \frac{2}{5}\eta^2}{85 + 102\eta + 34\eta^2}, \\ D_{eff} &= \frac{17U^2}{120D_r} \cdot \frac{136 + \eta}{136 + 85\eta}. \end{aligned} \tag{2.31}$$

The prefactor $\frac{17U^2}{120D_r}$ was chosen to make limiting case where $\eta \to 0$ result in $D_{eff}, D^R_{eff} \to \frac{17U^2}{120D_r}$. When $\eta \to \infty$ we have $D_{eff}, D^R_{eff} \to 0.01\frac{17U^2}{120D_r}$. A plot comparing the effective diffusion constants normalized so that both D_{eff} and D^R_{eff} both approach 1 as $\eta \to 0$, figure 2.8, shows that restricting transitions limits diffusivity in the intermediate range of η, with free transitions resulting in a maximum increase in diffusion of 19% over restricted transitions. Even though we do not match transition statistics exactly, this example shows that we are able to effectively approximate restricted systems. Our slight overestimate of diffusivity is outweighed by the ease of use our model provides.

2.7 Conclusions

We have formulated a model for the dispersal of swimmers undergoing stochastic switches between multiple speeds, in arbitrary dimensions. Our model can approximate the effective diffusion coefficient for swimmers jumping between any number of velocities. Our result shows that a reliable diffusion coefficient cannot be obtained by simply taking the mean speed and adding noise. Instead, each individual velocity directly affects diffusivity. As more observations of living organisms are collected and analyzed, we may find the velocity distributions to show numerous distinct peaks. Our model provides a quick and useful tool to predict the effective diffusion constant in these cases.

Comparing our model with previous works we have shown the model's flexibility. We have observed that, despite having the same velocity distribution, the dispersal rate is faster with stochastic rather than deterministic changes in velocity, and that the dispersal rate can slow down by restricting certain velocity jumps. These findings imply that great care is needed in predicting dispersal rates. The exact rate of long-term dispersal can depend sensitively on the nature of short-term velocity fluctuations. Nonetheless, the dispersal rate can be approximated reasonably well by a simplified model as demonstrated here.

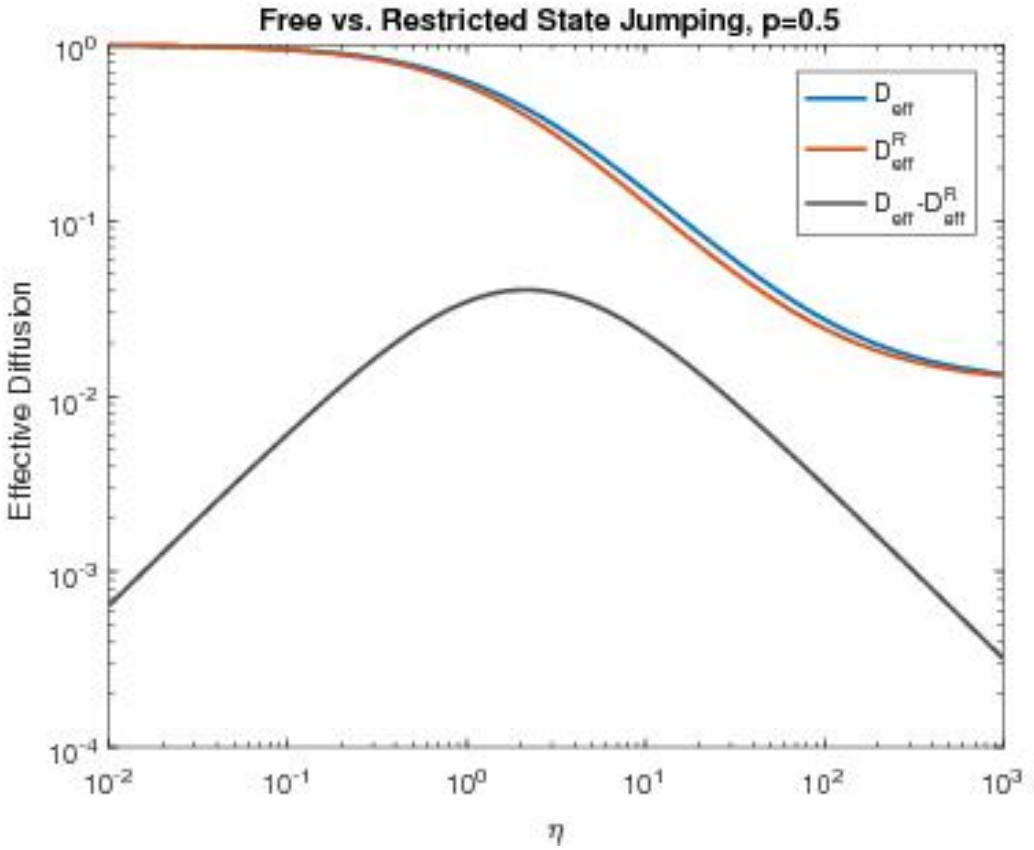

Figure 2.8: Comparison between the original model of three-speed swimmers [32] with restricted jumping (Figure 6) and our approximate model with free jumping (Figure 7). Minimal difference between the two models implies that swimmers with restricted changes can be reasonably well approximated by swimmers changing freely between additional states with an effective switch rate.

CHAPTER 3
BOUNDS ON CHEMICAL SIGNALING AND SENSING IN LAMINAR FLOW

3.1 Theoretical Background

Before introducing the chaser we must know the concentration field of an instantaneous point release over time. This will also provide a basis for solutions of the moving source model. We describe concentration at a position $x \in \mathbb{R}^n$ and time t by a function $c(x,t)$. From Fick's law, which states flux is proportional to and opposes concentration gradient, we find $c(x,t)$ obeys the standard diffusion equation with diffusion coefficient D,

$$c_t(x,t) = D\Delta c(x,t). \tag{3.1}$$

The following fundamental solution to equation 3.1 can be found by standard methods such as self-similarity or a Laplace transform, [19] [13] [46] [5] [4] [12].

$$c_\delta(x,t) = \frac{1}{(4\pi Dt)^{n/2}} e^{\frac{-|x|^2}{4Dt}}. \tag{3.2}$$

Linearity of equation 3.1 allows the use of superposition and equation 3.2 to obtain spacial and temporal concentration profiles from varied release patterns. Note that c_δ has units of inverse volume. Using either mass, molecular count, or volume as an initial condition will result in $c(x,t)$ describing either mass, molecular count, or proportion of volume over time.

3.1.1 Fundamental Solution Derivation

We will follow the development in [19], as it is mathematically straight forward. We will find a solution for $c_t(x,t) = \Delta c(x,t)$, which can be transformed back to the original equation by rescaling time. We start by assuming our solution has the form $c(x,t) = \frac{1}{t^\alpha} v(\frac{x}{t^\beta})$. Setting $y = \frac{x}{t^\beta}$ we have

$$\begin{aligned} \frac{\partial}{\partial t}\left(\frac{1}{t^\alpha} v\left(\frac{x}{t^\beta}\right)\right) &= -\alpha t^{-(\alpha+1)} v(y) - \beta t^{-(\beta+1)} y \cdot Dv(y) \\ \Delta\left(\frac{1}{t^\alpha} v\left(\frac{x}{t^\beta}\right)\right) &= t^{-(\alpha+2\beta)} \Delta v(y). \end{aligned} \tag{3.3}$$

Substituting equation 3.3 into 3.1 we get

$$\alpha t^{-(\alpha+1)} + \beta t^{-(\alpha+1)} y \cdot Dv(y) + t^{-(\alpha+2\beta)} \Delta v(y) = 0. \tag{3.4}$$

To divide out the t terms we set $\beta = \frac{1}{2}$. We then assume radial symmetry, $v(y) = w(|y|)$, which results in

$$\alpha w(r) + \frac{1}{2} r w'(r) + \frac{n-1}{r} w'(r) + w''(r) = 0 \tag{3.5}$$

Substituting $\alpha = \frac{n}{2}$, we get

$$\begin{aligned} \frac{n}{2} w(r) + \frac{1}{2} r w'(r) + \frac{n-1}{r} w'(r) + w''(r) &= 0 \\ (n-1) r^{-n} w'(r) + r^{n-1} w''(r) + \frac{1}{2}(n r^{n-1} w(r) + r^n w'(r)) &= 0 \\ (r^{n-1} w')' + \frac{1}{2}(r^n w)' &= 0 \\ r^{n-1} w' + \frac{1}{2} r^n w &= a \end{aligned} \tag{3.6}$$

Assuming $\lim_{r \to \infty} w, w' = 0$, we have $a = 0$. Thus

$$\begin{aligned} w'(r) &= -\frac{1}{2} r w(r) \\ w(r) &= b e^{-\frac{r^2}{4}} \\ c(x,t) &= \frac{b}{t^{\frac{n}{2}}} e^{-\frac{|x|^2}{4t}} \end{aligned} \tag{3.7}$$

Setting b so that integration over space gives 1 results in

$$c(x,t) = \frac{1}{(4\pi t)^{\frac{n}{2}}} e^{-\frac{|x|^2}{4t}} \tag{3.8}$$

After re-scaling time by substituting Dt for t we arrive at the fundamental solution.

3.1.2 Instant Release at a Point

To model a finite, instantaneous point release of strength c_0 at $t = 0$ our initial condition is $c(x, 0) = c_0 \delta(x)$. For $n = 1, 2, 3$ this models either a plane, line, or point source in 3-d. Since the solution has radial symmetry we set $r = |x| \in \mathbb{R}$ and obtain the solution

$$c(r,t) = \int_{\mathbb{R}^3} c_0 \delta(x) c_\delta(x,t) dx = \frac{c_0}{(4\pi D t)^{n/2}} e^{\frac{-r^2}{4Dt}}. \tag{3.9}$$

Detection of Absolute Concentration

We will assume that a "hunter" can detect the chemical only above some absolute concentration c_d. With this assumption, a stationary hunter positioned far enough away from the origin may never detect the release. This is demonstrated in figure 3.1. Numbers used are $D = 10^{-3}[\frac{mm^2}{s}]$ [43] [31] [63] [47] [45] [5] [30], $\frac{c_0}{c_d} = 20mm^3$ [58], which are reasonable for the open ocean, and have been seen to result in clusters of bacteria a few millimeters in diameter forming over the course of 140 seconds and lasting approximately ten minutes [58] [8].

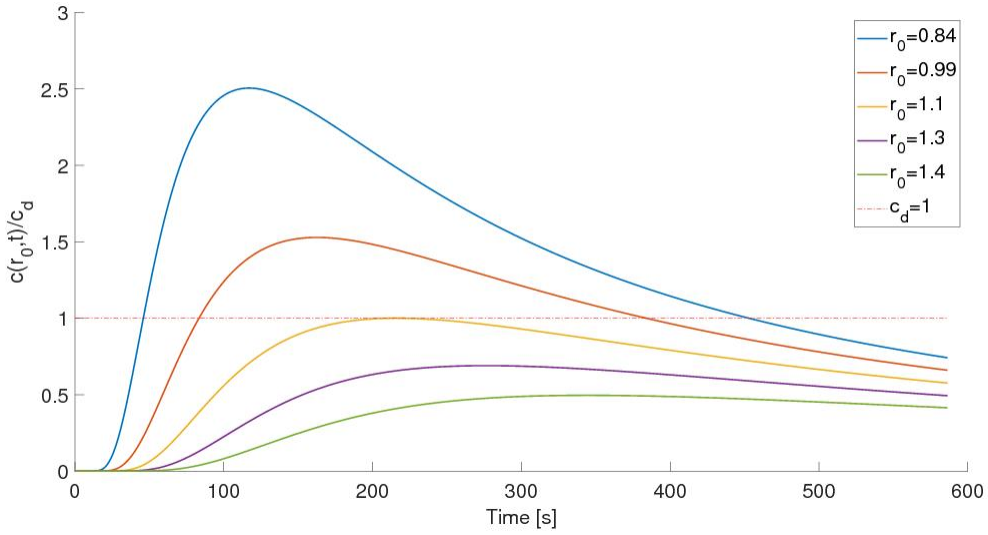

Figure 3.1: Concentration profiles traced through time for given initial distance r_0 $[mm]$ from a point source of strength $\frac{c_0}{c_d} = 20mm^3$ in 3D. Since the top two curves rise above c_d the chasing swimmer can detect the chemical release, lower curves represent swimmers that are too far away, and unable detect the chemical.

Once the hunter detects the signal it's goal is to reach the location of the source. Here a filter feeder has access to the most concentrated nutrients, or a tasty organism. The hunter's ability to do this depends on its motility. There is a critical radial approach speed it must attain either through direct chemotaxis or run and tumble induced drift. If it cannot move fast enough the signal could diffuse to unusable levels and no longer be of use.

Let's assume our hunter can detect the signal. Symbolically this is when $c(x,t) \geq c_d$. Using

equation (3.9) we can find a critical radius inside of which the signal is detectable,

$$r_c(t) = \sqrt{-4Dt \ln\Big(\frac{c_d}{c_0}(4\pi Dt)^{\frac{n}{2}}\Big)}. \tag{3.10}$$

Two zeros are found: one when $t = 0$, and the other at

$$t_f = \frac{1}{4\pi D}\Big(\frac{c_0}{c_d}\Big)^{\frac{2}{n}}. \tag{3.11}$$

Only between these times can the signal be detected by the chaser.

After taking a temporal derivative,

$$\begin{aligned}
\dot{r}_c(t) =& \frac{n}{2}\Big(-4Dt\ln\Big(\frac{c_d}{c_0}(4\pi Dt)^{\frac{n}{2}}\Big)\Big)^{-\frac{1}{2}} \\
&\cdot\Big(-4D\ln\Big(\frac{c_d}{c_0}(4\pi Dt)^{\frac{n}{2}}\Big) - 4Dt\frac{c_0}{c_d(4\pi Dt)^{n/2}}\frac{c_d}{c_0}(4\pi D)^{n/2}(\frac{n}{2}t^{\frac{n}{2}-1})\Big) \\
=& \frac{n}{2}\Big(-4Dt\ln\Big(\frac{c_d}{c_0}(4\pi Dt)^{\frac{n}{2}}\Big)\Big)^{-\frac{1}{2}}\Big(-4D\ln\Big(\frac{c_d}{c_0}(4\pi Dt)^{\frac{n}{2}}\Big) - 4Dtt^{-\frac{n}{2}}(\frac{n}{2}t^{\frac{n}{2}-1})\Big) \\
=& -2D\Big(-4Dt\ln\Big(\frac{c_d}{c_0}(4\pi Dt)^{\frac{n}{2}}\Big)\Big)^{-\frac{1}{2}}\Big(\ln\Big(\frac{c_d}{c_0}(4\pi Dt)^{\frac{n}{2}}\Big) + \frac{n}{2}\Big),
\end{aligned} \tag{3.12}$$

and setting $\dot{r}_c(t) = 0$ we find

$$\begin{aligned}
\ln\Big(\frac{c_d}{c_0}(4\pi Dt)^{\frac{n}{2}}\Big) + \frac{n}{2} &= 0 \\
\frac{c_d}{c_0}(4\pi Dt)^{\frac{n}{2}} &= e^{-\frac{n}{2}} \\
t &= \Big(\frac{c_0}{c_d(4\pi D)^{\frac{n}{2}}}e^{-\frac{n}{2}}\Big)^{\frac{2}{n}} \\
t_{max} &= \frac{1}{4\pi De}\Big(\frac{c_0}{c_d}\Big)^{\frac{2}{n}}.
\end{aligned} \tag{3.13}$$

Inserting this in equation 3.10 gives

$$\begin{aligned} r_{max} &= r_c(t_{max}) \\ &= \sqrt{-4D\frac{1}{4\pi De}\left(\frac{c_0}{c_d}\right)^{\frac{2}{n}} \ln\left(\frac{c_d}{c_0}(4\pi D\frac{1}{4\pi De}\left(\frac{c_0}{c_d}\right)^{\frac{2}{n}})^{\frac{n}{2}}\right)} \\ &= \sqrt{-\left(\frac{c_0}{c_d}\right)^{\frac{2}{n}}\frac{1}{\pi e}\ln\left(\frac{c_d}{c_0}\frac{c_0}{c_d}e^{-\frac{n}{2}}\right)} \\ &= \sqrt{\frac{n}{2\pi e}}\left(\frac{c_0}{c_d}\right)^{\frac{1}{n}} \end{aligned} \tag{3.14}$$

to find a max of equation (3.10) we find that our critical chaser detects the chemical at maximum radius and time

$$(r_{max}, t_{max}) = (\sqrt{\frac{n}{2\pi e}}\left(\frac{c_0}{c_d}\right)^{\frac{1}{n}}\ ,\ \frac{1}{4\pi De}\left(\frac{c_0}{c_d}\right)^{\frac{2}{n}}). \tag{3.15}$$

Assuming our hunter is located at (r_{max}, t_{max}) when it detects the signal, we can find the critical radial speed it must travel to be

$$v_c = \frac{2D\sqrt{2n\pi e}}{e-1}\left(\frac{c_d}{c_0}\right)^{\frac{1}{n}}, \tag{3.16}$$

which is the slope magnitude of the line connecting (r_{max}, t_{max}) and $(0, t_f)$.

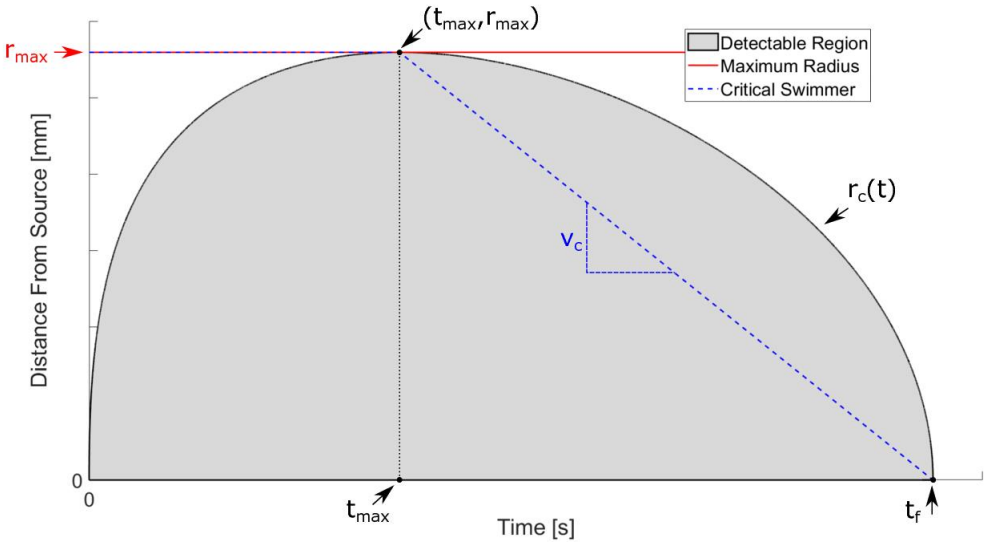

Figure 3.2: Typical detectable region over time for a 3-D point source with variable names indicated.

From these equations we see that for a point source doubling the initial chemoattractant release will increase the maximum radius by 26%, doubling the maximum detectable volume, and increase

the time the signal is detectable by 59%. A graph of the typical critical region with maximum radius over time can be found in figure 3.2.

Detection of Temporal Changes

It may be the case that a hunter can sense absolute concentration, but is unable to sense directional information directly. This could be due to sensor configuration or small size. After detecting a chemical signal these organisms must move and measure concentration changes over time to reorient properly. In the optimum case where the swimmer moves radially inward toward the source at speed U we have $\dot{r}(t) = -U$. First we compute

$$\begin{aligned} c_t(r,t) &= \frac{c_0}{(4\pi D)^{\frac{n}{2}}} e^{\frac{r^2}{4Dt}} \Big(-\frac{n}{2} t^{-\frac{n}{2}} t^{-1} + t^{-\frac{n}{2}} \frac{r^2}{4Dt^2} \Big) \\ &= \Big(\frac{r^2}{4Dt^2} - \frac{n}{2t} \Big) \frac{c_0}{(4\pi Dt)^{\frac{n}{2}}} e^{\frac{r^2}{4Dt}} \\ &= \Big(\frac{r^2 - 2nDt}{4Dt^2} \Big) c(x,t). \end{aligned} \tag{3.17}$$

It will take a couple steps to get at $c_r(x,t)$;

$$\begin{aligned} c_{x_i}(x,t) &= \frac{c_0}{(4\pi Dt)^{\frac{n}{2}}} e^{\frac{r^2}{4Dt}} \Big(\frac{-1}{4Dt} 2x_i \Big), \\ &= \frac{-2x_i}{4Dt} c(r,t) \\ \Delta c(r,t) &= x \ \frac{-2}{4Dt} c(r,t), \\ c_r(r,t) &= \Delta c \cdot \frac{x}{r} \\ &= \frac{-2x \cdot x}{4Dtr} c(r,t) \\ &= \frac{-2r}{4Dt} c(r,t). \end{aligned} \tag{3.18}$$

The temporal change in concentration is given by

$$\begin{aligned} \frac{D}{Dt} c(r(t),t) &= \dot{r} c_r(r,t) + c_t(r,t) \\ &= \Big(\frac{r^2 + 2Utr - 2nDt}{4Dt^2} \Big) c(r,t). \end{aligned} \tag{3.19}$$

From this equation we see that sensitivity increases with radial speed. We assume, as before, that this signal must be larger than some δ_m before it is detected. Symbolically this is when $\frac{D}{Dt} c(r(t),t) > \delta_m$.

For very small radial distances from the source we see that the experienced gradient is negative, due to temporal changes. The signal strength increases with radial distance until it becomes larger than δ_m. We label this location as r_i, the inner boundary of temporal stimulus. This region near the source where directional information is unavailable explains why bacteria in [8] were seen to overrun the source with high probability. As temporal stimulus decreases exponentially with r^2, there will be a larger r_o, the outer boundary of temporal stimulus, where the signal once again becomes undetectable. Additional information is only available in a donut shaped region around the nutrient source, visualized in figure 3.3, where we use a swimming speed of $v_s = 100\frac{\mu m}{s}$ [58].

The model presented in [27] arrives at similar results after discussing in detail molecular encounters and sensory timescales due to boundary layers. This information is interesting in its own right. It can be modified to explain some organisms increasing sensitivity with speed through a process called log sensing. However, it complicates the mathematical side of the analysis to nearly indigestible levels. The approach taken here explains the same observed behaviors through a much simpler exposition.

3.1.3 Moving Source With Continuous Release

Motivated by copepods, we will assume there are two objects, a source and a chaser. The source continuously releases a chemical compound. With our coordinates fixed on the source, we describe the chemical concentration at a point $x \in \mathbb{R}^3$ and time $t \in \mathbb{R}$ by the function $c(x,t)$. Assuming the concentration at the source is c_0 we can describe the chemical trail produced by a source moving with constant velocity vector $-\underline{u} \in \mathbb{R}^3$ by the advection-diffusion equation

$$\frac{\partial c}{\partial t} + \underline{u} \cdot \nabla c = D\Delta c, \tag{3.20}$$

where ∇ is the standard gradient operator and Δ is the Laplacian [5], [13], [19], [12], [4], and [46]. Note that this equation describes the trailing chemical plume in the source frame, and is equivalent to a stationary source in uniform flow field, which could also be used to describe a smokestack, or an organic seep. We then introduce the chaser, who will orient up concentration gradient and swim at speed v when it can detect the chemical.

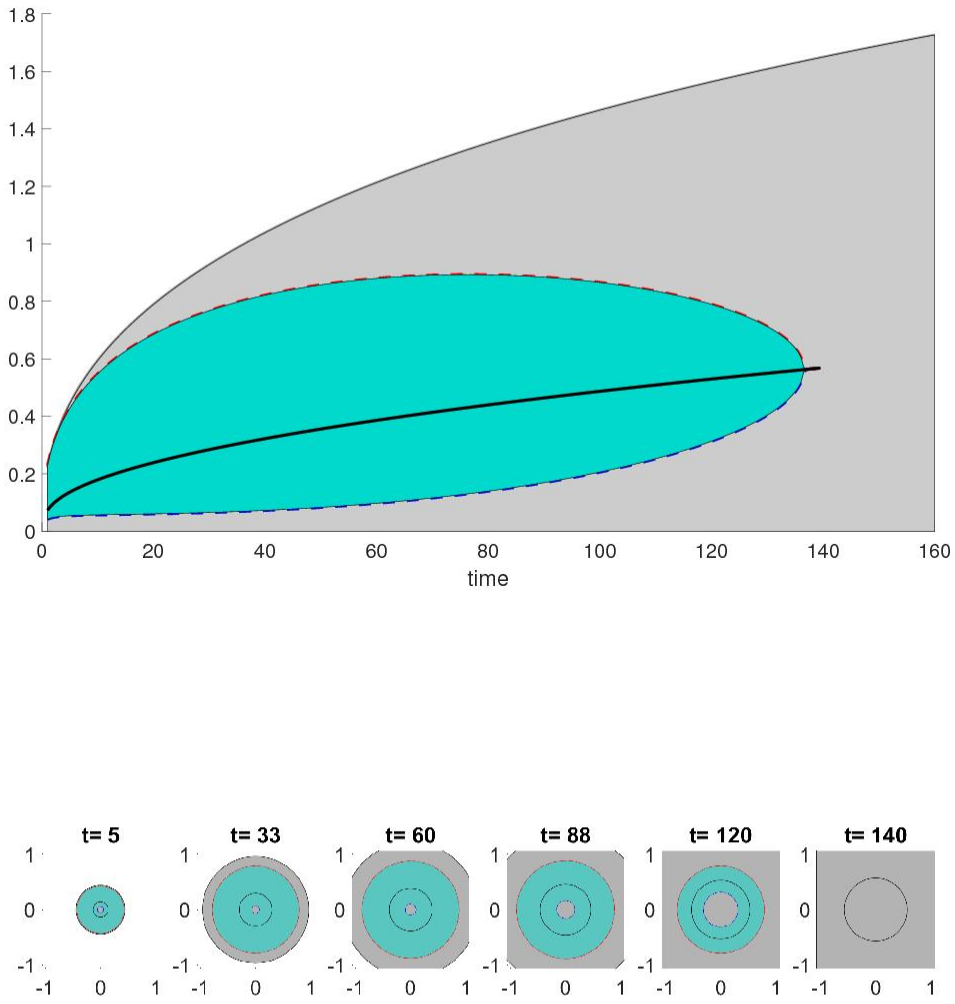

Figure 3.3: Top: Detectable regions along with signal max for concentration mediated detection describe by r_c, and motility based sensing at $u = 100\frac{\mu m}{s}$. Bottom: The region where motion gives directional information over time.

General Chemotactic Chase Result

Suppose our chaser can detect the chemical at any concentration. If the chaser orients itself up gradient and swims at speed v then his swimming velocity vector, in the source frame, is given by

$$\underline{s} = v\Big(\frac{\nabla c}{|\nabla c|}\Big) + \underline{u}. \tag{3.21}$$

In a reasonable scenario the chaser must be able to swim faster than the source, otherwise capture would be impossible. Symbolically this means $|\underline{u}| < v$. Since $|\underline{u} \cdot \nabla c| \leq |\underline{u}||\nabla c| < v|\nabla c|$,

$$\nabla c \cdot s = (v|\nabla c| - \underline{u} \cdot \nabla c) > 0. \tag{3.22}$$

The change in concentration along the chasers path is always positive, so a concentration orienting chaser will always find a local concentration maximum.

In the case of a source moving in a near straight line in the low Reynold's number regime the source will always be the only local max, so capture is inevitable. The relevant questions become about timescales and distances relevant to detection. For a detection to result in a non-capture [17] [2] a local maximum would need to appear away from the source. This could be a result of high curvature of source path, uneven release of chemical, non-constant swimming speed, or mixing due to background flow. In any of these cases a competent chaser would need to recognize that it has found a false source, then perform a search in hope of re-connecting with the trail.

Trailing Plume Analysis

In a given time period we expect our source to move a distance on the order of u. We also expect our chemical trail to disperse a distance on the order of $\frac{D}{L}$, where L is our chosen length scale. These timescales are compared by the Péclet number $Pe = \frac{u}{D/L} = \frac{uL}{D}$. If $Pe \gg 1$ advection dominates diffusion in the x_1 direction, so we can neglect this diffusive term. We will assume this is the case, and that our trailing plume has settled into a steady state. Subscripts denoting partial derivatives, our full advection-diffusion equation 3.20 reduces to

$$uc_{x_1} = D(c_{x_2x_2} + c_{x_3x_3}), \tag{3.23}$$

as in [33], [13].

You may recognize this as equivalent to a point source in 2-D after variable changes $x_1 \to t$, $x_{i+1} \to x_i$, $D \to \frac{D}{u}$. Again from [19] we have fundamental solution in cylindrical coordinates with respect to x_1, with $r = |\langle x_2, x_3 \rangle|$.

$$c_\delta(x_1, r) = \left(\frac{u}{4\pi D x_1}\right) \exp\left(\frac{-r^2 u}{4D x_1}\right). \tag{3.24}$$

This solution has units $[m^{-2}]$. We proceed as before. The boundary condition is a constant point source at the origin, $c(0,a) = c_0\delta(a)$, where c_0 has units of either mass, molecular count, or volume per distance. This describes a source moving on the x_1-axis with speed u. If our source produces chemical at a rate $q\frac{[\cdot]}{s}$, the dot denoting chosen units, while swimming at $u\frac{mm}{s}$ we have $c_0 = \frac{q}{u}$. This produces the concentration profile

$$\begin{aligned} c(x_1, r) &= \int_{\mathbb{R}^2} c_0\delta(a)c_\delta(x_1, \langle x_2, x_3\rangle - a)dx_2, x_3 \\ &= \frac{q}{4\pi D x_1}\exp\big(\frac{-r^2 u}{4Dx_1}\big). \end{aligned} \tag{3.25}$$

From this boundary we can compute maximum distances from the center of the plume for detection of the chemical by the chaser, and timescales for capture after detection is achieved. To answer these questions and find the orientation of our up gradient chaser we compute

$$\begin{aligned} c_{x_1}(x_1, r) &= \Big(\frac{ur^2 - 4Dx_1}{4Dx_1^2}\Big)c(x_1, r), \\ c_{x_j}(x_1, r) &= -x_j\Big(\frac{u}{2Dx_1}\Big)c(x_1, r), \\ c_r(x_1, r) &= \nabla c \cdot \frac{(x_2, x_3)}{r} = \Big(\frac{-ur}{2Dx_1}\Big)c(x_1, r), \end{aligned} \tag{3.26}$$

Lets set a concentration detection threshold, $c_d\frac{[\cdot]}{m^3}$. Setting $c(x_1, r) = c_d$ and solving for r in terms of x_1 we can get a boundary region of detection defined by

$$r_c(x_1) = \sqrt{\frac{-4Dx_1}{u}\ln\Big(4\pi D x_1\big(\frac{c_d}{q}\big)\Big)}. \tag{3.27}$$

We can solve for the largest radial point by using our detectable boundary equation 3.27. Where $\frac{\partial}{\partial x_1}r_c = 0$ we have the maximum radius. This happens at

$$(x_{max}, r_{\max}) = \left(\frac{1}{4\pi De}\Big(\frac{q}{c_d}\Big), \sqrt{\frac{1}{\pi eu}\Big(\frac{q}{c_d}\Big)}\right) \tag{3.28}$$

which agrees with [33]. Setting $r^2 = 0$ in the boundary equation gives the furthest downstream detectable distance

$$x_{\text{end}} = \frac{1}{4\pi D}\Big(\frac{q}{c_d}\Big). \tag{3.29}$$

A schematic showing variable names and a cross section of the trailing plume is shown in figure 3.4.

The distance that the chemical trail is detectable is independent of swimming speed. So is

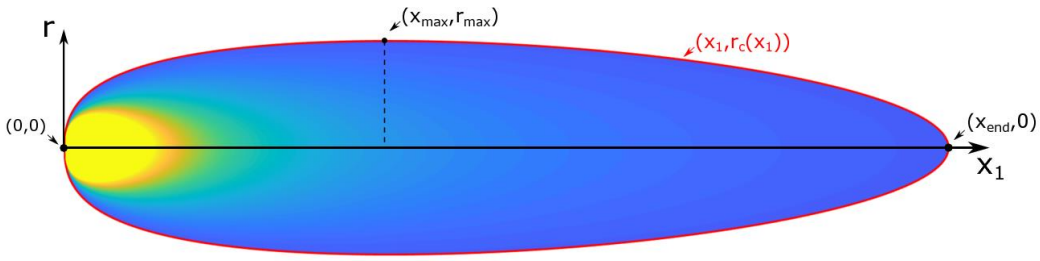

Figure 3.4: A cross section of the 3-D detectable plume created by a moving source with variable names denoting downstream distance and radial width indicated. Scale has been distorted for visual appeal.

the 'downstream' distance of the maximum radius. However, the maximum radius decreases with increasing speed as $u^{-1/2}$. Swimming faster actually decreases the size of the detectable signal. In the next section we discuss optimum setups for different chaser/source pairing. Once detection happens the maximum distance between the chaser and source is $x_{\max}$. Since most chases do not start at the end of the trail, and we are assuming high Pe, we get a course timescale of $\frac{x_{\max}}{v-|u|}$ describing time from detection to capture.

3.2 Discussion and Applications

3.2.1 Encouter Rates

Over time evolution has time to fine tune signaling and detection. A classic work on optimal pairings has concluded that fast predators are best suited for slow prey and slow moving ambush predators are better suited to harvest fast prey [22]. A spherical detection region of constant radius is assigned around organisms, and organisms are assumed to be uniformly distributed in space. This was meant to be a general model for all types of encounters. Since we have specific information about chemical signaling, we have an opportunity to do our own more specific optimization analysis and compare results. Using their work as motivation we provide analysis of pairwise encounters, focusing on chemically mediated signaling.

We will assume that organisms create and store a finite amount of chemical before releasing it into the environment. They then either release the chemical all in one location, or create a trailing plume until their chemical store is depleted. The chemical signal will be quite different whether the organism moves or stays still. We will use the models developed earlier to give an accurate

description of the resulting detectable regions. Then we discuss whether a signal by a moving or nearly stationary source is best suited for detection by a highly motile, or nearly stationary organism.

If the chaser is nearly stationary, like an ambush predator, a signal must pass through it's immediate surroundings to be detected. Here the volume swept by the chemical signal must include the observer for direction. We will denote this volume by V. Things change for an observer that is highly motile. The important figure is total swept surface area since such an observer could enter the detectable region from any angle at any time. We will denote swept surface area by S. Subscripts will be used to denote whether the source is considered to be nearly stationary, s, or moving, m. Optimum combinations along with relevant figures are summarized neatly in table 3.1.

Table 3.1: Relevant descriptive figures for chemically mediated encounters between organisms. Subscripts denote a stationary (s) or moving (m) source, while V and S denote volume and surface area respectively.

	Stationary Source	***Moving Source***
Slow Chaser	V_s	V_m
Fast Chaser	A_s	A_m

Let's denote the finite amount of chemical tracer by K. For our point source models this will be included as $c_0 = K$. The volume swept by a stationary source is simply the volume of the largest detectable sphere, which has radius r_{max} from equation 3.15, and is given by

$$V_s(K) = \frac{4}{3}\pi r_{max}^2 = \sqrt{\frac{3}{2\pi e^3}}\frac{K}{c_d} \approx 0.15\frac{K}{c_d}. \tag{3.30}$$

We assume in the moving source model that a steady state has been reached. Since we are neglecting diffusion along the path of the signaling organism this occurs at the time when the length of the plume has been traveled. Using equation 3.29 we compute this time to be

$$t_i = \frac{x_{end}}{u} = \sqrt{\frac{K}{4\pi u D c_d}}. \tag{3.31}$$

The organism must take at least this long to release its stored chemical for our model to be valid. Since our model has release rate q, and will release a chemical amount K over a period of t seconds we have

$$q = \frac{K}{t}. \tag{3.32}$$

The total volume swept is the volume of the plume added to the cylinder swept by the maximal

cross sectional area. This can be visualised in figure 3.4 by cutting at the line marked by r_{max} and extending the plume. We will need equations 3.27, 3.28, and 3.29 along with equations 3.31 and 3.32 above. For $t > t_i$ it is given by

$$\begin{aligned} V_m(K,t) &= \int_0^{x_{end}} \pi r_c(x_1)^2 dx_1 + (t-t_i)u\pi r_{max}^2 \\ &= \frac{K}{ec_d} - \frac{4-e}{16e\pi Du}\left(\frac{K}{tc_d}\right)^2, \end{aligned} \tag{3.33}$$

which is dependent not only on the amount of chemical, but also the time taken to release the chemical. From equation 3.33 we see that V_m has a maximum at t_i, and approaches a minimum value of $\frac{K}{ec_d}$ for large release times. The lengthening and thinning of the detectable signal balances nicely at large times to give this limit.

From equation 3.11 we know the signal is only above detectable levels until t_f seconds after release. With this and the critical radius formula 3.10 we compute the swept surface area for immediate release at a point as

$$A_s = \int_0^{t_f} 4\pi r_c(t)^2 dt = \frac{3}{8\pi D}\left(\frac{K}{c_d}\right)^{\frac{4}{3}}. \tag{3.34}$$

The swept surface area calculation for a moving source is only valid for release periods longer than t_i as we have assumed a steady state. Since our plume is long and slender in the high Pe scenario we also assume $\frac{dr_c(x_1)}{dx_1} \approx 0$. This approximation simplifies the surface area integral dramatically, allowing for an analytic solution. We will need equations 3.27, 3.29, 3.31, and 3.32. Once we have the surface area of the trailing plume we simply multiply by time to compute the swept area by a fully formed plume

$$A_m(K,t) \approx t\int_0^{x_{\text{end}}} 2\pi r_c(x_1) dx_1 = \frac{0.24}{D\sqrt{\pi ut}}\left(\frac{K}{c_d}\right)^{\frac{3}{2}}. \tag{3.35}$$

With these formulae we can make comparisons of what type of signal a chaser is most likely to detect. Slow, nearly stationary chasers are described by equations 3.33 and 3.30. We assume that once detection is made these organisms have the motility required to overtake and capture the source. However, they sit nearly still as a search strategy. As V_m increases with t we have $V_m(K,t) - V_s(K) \geq V_m(K,t_i) - V_s(K) = 0.1 > 0$. This means that a slow chaser is more likely to detect a moving source than a stationary one. An ambush style predator would be more likely to encounter fast moving prey then organisms that move very slowly.

Fast moving chasers will have encounter zones described by equations 3.35 and 3.34. Since A_m decreases with t we have $A_s(K) - A_m(K,t) \geq A_s(K) - A_m(K,t_i) \geq 0 \iff \frac{K}{c_d} \geq 8 * (\frac{D}{u})^3$. A moving source will only have a larger signal in cases where the deposited chemical has a very high diffusion constant. In these cases the time that a stationary signal is available is very short, and this is offset by the duration of a small moving source plume. In the open ocean $D \approx 10^{-3} \frac{mm^2}{s}$, $u < 100$, and $\frac{K}{c_d} \approx 10^2$. Thus for reasonable applications we have $A_s > A_m$. A fast chaser is more likely to encounter a stationary source than a moving one.

Our analysis confirms and extends the results of [22]. Whether a spherical region, or the more complicated region occupied by a chemical signal is used, fast/slow parings of source and chaser are most likely to encounter each other.

3.2.2 Applications

For what follows we use common value of diffusivity for organic molecules in water, $D = 10^{-3} \frac{mm^2}{s}$ [43] [31] [63] [47] [45] [5] [30].

To model a bacterium chasing a point release we assume that a nutrient patch is detectable for 10 minutes [8] [20]. Working backwards from equation 3.11 we find $\frac{c_0}{c_d} = (4\pi D t_f)^{3/2} = 20.7 mm^3$. Thus bacterium can typically detect nutrient plumes in the open ocean until they have decayed by a factor of 20. This gives a maximum detectable radius from equation 3.15 of $1.15mm$. The critical chemotactic velocity from equation 3.16 is $1.7 \frac{\mu m}{s}$, which is easily achievable by marine bacteria, which typically have chemotactic velocites of around $10 \frac{\mu m}{s}$ [56], [27].

In [45] T. Longicornis was observed following chemical trails left by discarded appendicularian houses. Houses were approximated as sinking sources with speed $1 \frac{mm}{s}$, leaking traceable chemicals at $q(r) = 1.5 \cdot 10^{-12} \frac{Mol}{s}$. Copepods were assumed to sense the chemical at $c_d = 10^{-14} \frac{Mol}{mm^3}$. Following speed was approximately $7 \frac{mm}{s}$ after detection. Trail length and width were observed to be about 35 mm and 2 mm respectably. This is dramatically different than our calculations predict from trail length. With $D = 10^{-3} \frac{mm^2}{s}$ we obtain $(x_{max}, r_{max}) = (5.4m, 4.64mm)$ and $x_{end} = 15m$. To match their length calculations the diffusion constant would have to be between 3 and 4 orders of magnitude larger.

The mating behavior of T. Longicornis was discussed in [63] [17] [64] [31]. T. Longicornis is 1mm in size, so we set $L = 1$ [17] [31]. Females cruise at about $6 \frac{mm}{s}$ [64] [17]. Males pursue at about $24 \frac{mm}{s}$ [64] [17]. Males first encounter females trail from a radial distance of within $2mm$ [64] [17].

Males detect trails as old as $10s$ [64] [17]. Trail were tracked for more than $10cm$ [64] [17]. Persuits were $0.4 - 3.67s$ [17] in duration. Using the maximum detected age of a trail as 10s, we approximate the detectable trail is 60mm long. From equation 3.28 we conclude that $\frac{q}{c_d} = \frac{6\pi}{25} \approx 0.75 \frac{mm^3}{s}$. This gives $(x_{max}, r_{max}, x_{end}) = (22mm, 0.12mm, 60mm)$.

3.3 Concluding Remarks

We have described the detectable region of both deposition at a point and continuous release by a moving source. Our analysis gives a detectable region based on an initial release and minimum detectable concentration. For a stationary signaling organism we find a minimal speed necessary to reach the source location before the signal decreases below detectable levels. This can be interpreted as either a minimum swimming speed, or as a minimum induced chemotactic drift. The additional information gained from motion explains the source overrun observed in [8]. This combined with our calculations for information gained from motion give a thorough overview of the signals passed from sources that move very slowly.

We then changed focus to a moving source. In the general case it was found that a competent chaser with the ability to orient up gradient is guaranteed capture once detection happens. Calculations describing the following plume were then provided, along with gradients. This gives sufficient information to predict capture time scales given information about the chemical released by the source, the chasers sensitivity, and the velocity both move at.

Once scent profiles were established we discussed what pairings would be most likely for signaling and chasing organisms. Our results parallel those of [22] in nearly all cases. We then applied our results to some real world data. Some long, slender plumes made by copepods were described, as well as the profiles experienced by bacteria chasing the nutrients released by lysed cells.

CHAPTER 4
CONCLUSIONS

In this dissertation we have analyzed the dispersal of organisms, and their ability to interact via chemically mediated signals. Our analysis of dispersal has resulted in an adaptable model that can be used as a test for future modeling works, or as a quick tool to obtain an effective diffusion constant for organisms. We have found that added diffusion from motion is influenced by the average velocity, and the average added dispersion from each individual velocity. The relative weight of these terms is tuned by the rate at which changes in velocity occur, fast switching adding more weight to the average velocity effect. Our comparisons with previous work have shown that deterministic velocity jumps, and restricting change statistics reduce overall dispersal compared to free velocity jumping between all available velocities. Our model provides an accurate estimate for added dispersal, and can be used to predict how fast a group of organisms will disperse given their velocity change statistics and a diffusion constant.

The models of chemical signaling provides a description of how organisms interact with their environment as well as each other. Signals are described based on the organism speed, chemical diffusion constant, and the sensitivity of the chasing organism's sensory organs. For interactions such as lysed cells being consumed by bacteria we have provided a model for the region that contains a detectable concentration as it evolves through time, and another model for the region where temporal comparisons give additional information. For organisms with direct access to the concentration gradient we have provided a calculation for the minimum necessary speed, whether direct or via chemotactic drift, that an organism must reach to find the epicenter of the chemical release before it falls below detectable levels. We have shown through examples that this velocity is easily achievable to most organisms. Our trailing plume model has provided an analysis of the courtship chase male copepods embark on when searching for a mate. We have shown that in ideal circumstances a male is guaranteed to find a female once detection is made. Comparisons with previous works have described the plume left by sinking marine snow, and female copepods. Both produce long slender plumes, narrow enough that a chasing organism cannot always fit fully inside them. Our two models were then used to show that fast and slow organisms were likely to end up paired as signaler and chaser. This parallels the results of [22] who used a general model for sensing rather than one made specifically for chemical signals. As with all scientific work, we have added a small amount of

knowledge and identified many avenues for future work.

The analysis has provided models general enough, and simple enough to be used as a backdrop for future research. The model for additional diffusion could be modified to accept more information as an input. Fluid interactions and direct interactions between swimmers are possible avenues. Some sensory information could also be used to modify the distribution that velocities are taken from. A combination of the two models presented here could be used to obtain a signal to detection ratio for bacteria around lysed cells. In [8] bacteria concentrations could be seen as organisms responding to a release, then diffusing via their normal swim strategy. If executed correctly this could provide a more accurate description than direct inference from bacterial density. Modification of the chemical signalling model to include information on background flow, and more complicated swim behaviors could serve to improve accuracy. Changes in speed could explain loss of path observed in copepods. As always with research there are avenues for improvement. We look forward to future investigation from whoever is interested.

BIBLIOGRAPHY

[1] Sonja Babel, B Ten Hagen, and Hartmut Löwen. Swimming path statistics of an active brownian particle with time-dependent self-propulsion. *Journal of Statistical Mechanics: Theory and Experiment*, 2014(2):P02011, 2014.

[2] Espen Bagøien and Thomas Kiørboe. Blind dating—mate finding in planktonic copepods. i. tracking the pheromone trail of centropages typicus. *Marine Ecology Progress Series*, 300:105–115, 2005.

[3] Greg M Barbara and James G Mitchell. Marine bacterial organisation around point-like sources of amino acids. *FEMS microbiology ecology*, 43(1):99–109, 2003.

[4] Grigory Isaakovich Barenblatt and Barenblatt Grigory Isaakovich. *Scaling, self-similarity, and intermediate asymptotics: dimensional analysis and intermediate asymptotics*, volume 14. Cambridge University Press, 1996.

[5] H C Berg. *Random Walks in Biology*. Princeton University Press, 1983.

[6] Howard C Berg and Edward M Purcell. Physics of chemoreception. *Biophysical journal*, 20(2):193–219, 1977.

[7] Nicholas Blackburn, Farooq Azam, and Åke Hagström. Spatially explicit simulations of a microbial food web. *Limnology and Oceanography*, 42(4):613–622, 1997.

[8] Nicholas Blackburn, Tom Fenchel, and Jim Mitchell. Microscale nutrient patches in planktonic habitats shown by chemotactic bacteria. *Science*, 282(5397):2254–2256, 1998.

[9] William H Bossert. Temporal patterning in olfactory communication. *Journal of theoretical biology*, 18(2):157–170, 1968.

[10] Tommaso Brotto, Denis Bartolo, and David Saintillan. Spontaneous flows in suspensions of active cyclic swimmers. *Journal of Nonlinear Science*, 25(5):1125–1139, 2015.

[11] Antonio Celani, Emmanuel Villermaux, and Massimo Vergassola. Odor landscapes in turbulent environments. *Physical Review X*, 4(4):041015, 2014.

[12] Edward A Codling, Michael J Plank, and Simon Benhamou. Random walk models in biology. *Journal of the Royal society interface*, 5(25):813–834, 2008.

[13] Gabriel T Csanady. *Turbulent diffusion in the environment*, volume 3. Springer Science & Business Media, 2012.

[14] Guido Dehnhardt, Björn Mauck, Wolf Hanke, and Horst Bleckmann. Hydrodynamic trail-following in harbor seals (phoca vitulina). *Science*, 293(5527):102–104, 2001.

[15] Francois Detcheverry. Non-poissonian run-and-turn motions. *EPL (Europhysics Letters)*, 111(6):60002, 2015.

[16] François Detcheverry. Generalized run-and-turn motions: From bacteria to lévy walks. *Physical Review E*, 96(1):012415, 2017.

[17] Michael H Doall, Sean P Colin, J Rudi Strickler, and Jeannette Yen. Locating a mate in 3d: the case of temora longicornis. *Philosophical Transactions of the Royal Society of London. Series B: Biological Sciences*, 353(1369):681–689, 1998.

[18] Masao Doi and Samuel Frederick Edwards. *The theory of polymer dynamics*, volume 73. oxford university press, 1988.

[19] Lawrence C Evans. Partial differential equations and monge-kantorovich mass transfer. *Current developments in mathematics*, 1997(1):65–126, 1997.

[20] Tom Fenchel. Microbial behavior in a heterogeneous world. *Science*, 296(5570):1068–1071, 2002.

[21] Peter JS Franks. Models of harmful algal blooms. *Limnology and Oceanography*, 42(5part2):1273–1282, 1997.

[22] Jeroen Gerritsen and J Rudi Strickler. Encounter probabilities and community structure in zooplankton: a mathematical model. *Journal of the Fisheries Board of Canada*, 34(1):73–82, 1977.

[23] Rodrigo J Goncalves and Thomas Kiørboe. Perceiving the algae: How feeding-current feeding copepods detect their nonmotile prey. *Limnology and Oceanography*, 60(4):1286–1297, 2015.

[24] Robert Großmann, Fernando Peruani, and Markus Bär. Diffusion properties of active particles with directional reversal. *New Journal of Physics*, 18(4):043009, 2016.

[25] L Haeggqwist, L Schimansky-Geier, IM Sokolov, and F Moss. Hopping on a zig-zag course. *The European Physical Journal Special Topics*, 157(1):33–42, 2008.

[26] WOLF Hanke, C Brucker, and HORST Bleckmann. The ageing of the low-frequency water disturbances caused by swimming goldfish and its possible relevance to prey detection. *Journal of Experimental Biology*, 203(7):1193–1200, 2000.

[27] Andrew M Hein, Douglas R Brumley, Francesco Carrara, Roman Stocker, and Simon A Levin. Physical limits on bacterial navigation in dynamic environments. *Journal of The Royal Society Interface*, 13(114):20150844, 2016.

[28] Andrew M Hein and Scott A McKinley. Sensing and decision-making in random search. *Proceedings of the National Academy of Sciences*, 109(30):12070–12074, 2012.

[29] Gerhard J Herndl. Ecology of amorphous aggregations(marine snow) in the northern adriatic sea. 2. microbial density and activity in marine snow and its implication to overall pelagic processes. *Marine ecology progress series. Oldendorf*, 48(3):265–275, 1988.

[30] Jan Heuschele and Erik Selander. The chemical ecology of copepods. *Journal of plankton research*, 36(4):895–913, 2014.

[31] Peter Hinow, J Rudi Strickler, and Jeannette Yen. Olfaction in a viscous environment: the "color" of sexual smells in temora longicornis. *The Science of Nature*, 104(5-6):46, 2017.

[32] Marius Hintsche, Veronika Waljor, Robert Großmann, Marco J Kühn, Kai M Thormann, Fernando Peruani, and Carsten Beta. A polar bundle of flagella can drive bacterial swimming by pushing, pulling, or coiling around the cell body. *Scientific reports*, 7(1):16771, 2017.

[33] George A Jackson and Thomas Kiørboe. Zooplankton use of chemodetection to find and eat particles. *Marine Ecology Progress Series*, 269:153–162, 2004.

[34] Houshuo Jiang, Thomas R Osborn, and Charles Meneveau. Chemoreception and the deformationof the active space in freely swimming copepods: A numerical study. *Journal of Plankton Research*, 24(5):495–510, 2002.

[35] Thomas Kiørboe. Mate finding, mating, and population dynamics in a planktonic copepod oithona davisae: there are too few males. *Limnology and Oceanography*, 52(4):1511–1522, 2007.

[36] Thomas Kiørboe, Espen Bagøien, and Uffe Høgsbro Thygesen. Blind dating—mate finding in planktonic copepods. ii. the pheromone cloud of pseudocalanus elongatus. *Marine Ecology Progress Series*, 300:117–128, 2005.

[37] Thomas Kiørboe and George A Jackson. Marine snow, organic solute plumes, and optimal chemosensory behavior of bacteria. *Limnology and Oceanography*, 46(6):1309–1318, 2001.

[38] Thomas Kiørboe, Helle Ploug, and Uffe H Thygesen. Fluid motion and solute distribution around sinking aggregates. i. small-scale fluxes and heterogeneity of nutrients in the pelagic environment. *Marine Ecology Progress Series*, 211:1–13, 2001.

[39] MAR Koehl, JA Strother, MA Reidenbach, JR Koseff, and MG Hadfield. Individual-based model of larval transport to coral reefs in turbulent, wave-driven flow: behavioral responses to dissolved settlement inducer. *Marine Ecology Progress Series*, 335:1–18, 2007.

[40] Niko Komin, Udo Erdmann, and Lutz Schimansky-Geier. Random walk theory applied to daphnia motion. *Fluctuation and Noise Letters*, 4(01):L151–L159, 2004.

[41] Don A Krasky and Daisuke Takagi. Diffusion of swimmers jumping stochastically between multiple velocities. *Journal of Statistical Mechanics: Theory and Experiment*, 2018(10):103201, 2018.

[42] Eric Lauga. Enhanced diffusion by reciprocal swimming. *Physical review letters*, 106(17):178101, 2011.

[43] John T Lehman and Donald Scavia. Microscale nutrient patches produced by zooplankton. *Proceedings of the National Academy of Sciences*, 79(16):5001–5005, 1982.

[44] Petra H Lenz, Daisuke Takagi, and Daniel K Hartline. Choreographed swimming of copepod nauplii. *Journal of The Royal Society Interface*, 12(112):20150776, 2015.

[45] Fabien Lombard, Marja Koski, and Thomas Kiørboe. Copepods use chemical trails to find sinking marine snow aggregates. *Limnology and Oceanography*, 58(1):185–192, 2013.

[46] Vicenç Méndez, Daniel Campos, and Frederic Bartumeus. *Stochastic foundations in movement ecology*. Springer, 2014.

[47] Paul Moore and John Crimaldi. Odor landscapes and animal behavior: tracking odor plumes in different physical worlds. *Journal of marine systems*, 49(1-4):55–64, 2004.

[48] Ran Nathan, Wayne M Getz, Eloy Revilla, Marcel Holyoak, Ronen Kadmon, David Saltz, and Peter E Smouse. A movement ecology paradigm for unifying organismal movement research. *Proceedings of the National Academy of Sciences*, 105(49):19052–19059, 2008.

[49] Anke Ordemann, Gabor Balazsi, and Frank Moss. Pattern formation and stochastic motion of the zooplankton daphnia in a light field. *Physica A: statistical mechanics and its applications*, 325(1-2):260–266, 2003.

[50] Peter J Ortoleva and John Ross. Penetration of boundary perturbations in unstable chemical systems. *The Journal of Chemical Physics*, 56(1):287–292, 1972.

[51] Gustav-Adolf Paffenhöfer and Houshuo Jiang. Comment: On phytoplankton perception by calanoid copepods. *Limnology and Oceanography*, 61(4):1163–1168, 2016.

[52] Grigorios A Pavliotis. Stochastic processes and applications, 2014.

[53] Fernando Peruani and Luis G Morelli. Self-propelled particles with fluctuating speed and direction of motion in two dimensions. *Physical review letters*, 99(1):010602, 2007.

[54] Pawel Romanczuk, Markus Bär, Werner Ebeling, Benjamin Lindner, and Lutz Schimansky-Geier. Active brownian particles. *The European Physical Journal Special Topics*, 202(1):1–162, 2012.

[55] Lutz Schimansky-Geier, Udo Erdmann, and Niko Komin. Advantages of hopping on a zig-zag course. *Physica A: Statistical Mechanics and its Applications*, 351(1):51–59, 2005.

[56] Roman Stocker. Marine microbes see a sea of gradients. *science*, 338(6107):628–633, 2012.

[57] Daisuke Takagi, Adam B Braunschweig, Jun Zhang, and Michael J Shelley. Dispersion of self-propelled rods undergoing fluctuation-driven flips. *Physical review letters*, 110(3):038301, 2013.

[58] John R Taylor and Roman Stocker. Trade-offs of chemotactic foraging in turbulent water. *Science*, 338(6107):675–679, 2012.

[59] Matthias Theves, Johannes Taktikos, Vasily Zaburdaev, Holger Stark, and Carsten Beta. A bacterial swimmer with two alternating speeds of propagation. *Biophysical journal*, 105(8):1915–1924, 2013.

[60] Peter Tiselius, Enric Saiz, and Thomas Kiørboe. Sensory capabilities and food capture of two small copepods, paracalanus parvus and pseudocalanus sp. *Limnology and Oceanography*, 58(5):1657–1666, 2013.

[61] Atsushi Tsuda and Charles B Miller. Mate-finding behaviour in calanus marshallae frost. *Philosophical Transactions of the Royal Society of London. Series B: Biological Sciences*, 353(1369):713–720, 1998.

[62] Christian Weber, Igor M Sokolov, and Lutz Schimansky-Geier. Active particles forced by an asymmetric dichotomous angle drive. *Physical Review E*, 85(5):052101, 2012.

[63] DR Webster and MJ Weissburg. The hydrodynamics of chemical cues among aquatic organisms. *Annual Review of Fluid Mechanics*, 41:73–90, 2009.

[64] Marc J Weissburg, MH Doall, and Jeannette Yen. Following the invisible trail: kinematic analysis of mate-tracking in the copepod temora longicornis. *Philosophical Transactions of the Royal Society of London. Series B: Biological Sciences*, 353(1369):701–712, 1998.

[65] Jeannette Yen and Rachel Lasley. Chemical communication between copepods: finding the mate in a fluid environment. In *Chemical communication in crustaceans*, pages 177–197. Springer, 2010.